Benefits of multi-target and self-supervised LSTM models for water quantity and quality

Jean-Paul Brede[1], Pia Ebeling[2], Jens Kiesel[3], Ralf Loritz[1]

[1] Institute for Water and Environment, Karlsruhe Institute of Technology (KIT), Karlsruhe 76131, Germany
[2] Department of Hydrogeology, Helmholtz Centre for Environmental Research – UFZ, Leipzig 04318, Germany
[3] Stone Environmental, 535 Stone Cutters Way, 05602 Montpelier (VT), USA

Correspondence to: Jean-Paul Brede ~~()~~(jean-paul.brede@kit.edu) and Ralf Loritz ~~()~~(ralf.loritz@kit.edu)

Abstract. Deep learning has become a standard tool for streamflow ~~modeling~~modelling, but its application to water quality remains challenging due to sparse, irregular, and noisy in-situ observations. Yet, water-quality variables are tightly linked to discharge and to each other through shared hydrological and biogeochemical controls, suggesting that jointly ~~modeling~~modelling water quantity and quality may help compensate for limited data availability. In this study, we compare single-target, multi-target, and self-supervised LSTM models for the joint simulation of discharge and six water-quality variables (NO_3-N, PO_4-P, DO, DOC, EC, and WT) across 408 German catchments. Our results highlight that extending the ~~baseline~~LSTM from single-target discharge prediction to jointly predicting discharge and all six water-quality variables does not substantially degrade discharge performance (across all baseline configurations, median ~~KGE'~~KGE′ = 0.84–0.87) and yields median ~~KGE'~~KGE′ values between 0.~~35~~40 (PO_4-P) and 0.~~94~~95 (WT) for the water-quality targets. Interestingly, learning discharge as a co-target ~~consistently outperforms models that use~~matches or exceeds the performance of using observed discharge as an additional input~~, indicating~~ for five of the six water-quality variables, with the clearest gain for DOC (ΔKGE′ = +0.05). This indicates that jointly learning water quantity and quality ~~is~~can be more effective than using discharge as a predictor. A variable-averaged loss function is key to balance the strongly uneven observation densities of discharge and water-quality variables. Building on this multi-target framework, we further explore whether an alternative training strategy based on self-supervised learning can better exploit the incomplete and heterogeneous nature of environmental observations. Our evaluation reveals that the ~~self-supervised~~LSTM yields a level of predictive skill comparable to the multi-target supervised ~~baseline~~~~baseline~~LSTM under inference conditions restricted to meteorological drivers~~, while effectively leveraging cross-variable dependencies to enhance PO_4-P~~ and ~~DO reconstructions~~ when contextual water-quality data ~~are~~is provided. Thus, while matching the baseline's skill, the self-supervisedLSTM gains versatility, as a single model can be applied to many different combinations of available input data without retraining. Besides showcasing the strong performance of LSTMs in water-quality simulations with sparse and irregular data, our results demonstrate that multi-target learning provides an effective framework for coupled water quantity–quality ~~modeling~~modelling, while self-supervised learning offers additional flexibility for exploiting incomplete and heterogeneous environmental observations~~, yielding predictive skill comparable to, and in some~~

~~cases exceeding, that of calibrated process-based water-quality models and supporting the use of LSTMs as a scalable alternative for regional water quality simulation in data-sparse environments.~~.

1 Introduction

Deep learning (DL) has become an effective approach for hydrological ~~modeling~~modelling, offering a data-driven complement to traditional process-based methods. Particularly when trained on large-sample datasets, DL models can provide reliable water quantity estimates that often match or exceed the performance of conceptual benchmarks (e.g.~~,~~, Acuña Espinoza et al., ~~2024~~2025; Kratzert et al., 2019). Reflecting the field's rapid progress, these advancements are already being integrated into regional and global systems for operational flood and drought forecasting (Nearing et al., 2024). In contrast, the uptake of DL in water-quality (WQ) ~~modeling~~modelling has been slower (Zhi et al., 2024), partially due to the nature of the available data. Unlike water-quantity variables such as discharge or groundwater levels, which are typically observed ~~with~~automatically and at a high frequency ~~and automated~~, water-quality measurements are often sparse and irregular in time. Many observations are based on grab sampling, which can miss short-lived but extreme concentration peaks (Rathjens et al., 2023). In addition, measurement uncertainties are often higher due to laboratory analyses, detection limits, and sample handling. As a result, the limited temporal density, uneven coverage, and measurement uncertainties constrain the amount of information available about relevant processes for model training and evaluation, which poses a key challenge for any data-driven model.

Despite these challenges, the complexity of water-quality dynamics may also create opportunities for DL-based approaches (Zhi et al., 2024). Water-quality processes are governed by hydrological, biogeochemical, and anthropogenic interactions that vary across space and time, with solute transport and transformation controlled by factors such as land use (Vaughan et al., 2017), soil or storage-related properties (Musolff et al., 2015), as well as flow paths, temperature, redox conditions, and biological activity (McClain et al., 2003). These interactions create strong dependencies between variables, for example, nitrate, iron, phosphorus, and dissolved organic carbon are linked by redox conditions (Musolff et al., 2017), while temperature and discharge shape seasonal and event-driven dynamics in concentrations (Ebeling et al., 2021; Zhi et al., 2023). For instance, nitrate concentrations often increase with streamflow during seasonal wet periods and storm events due to leaching and runoff (Ebeling et al., 2021; Minaudo et al., 2019), while dissolved oxygen is closely linked to water temperature with seasonal minima during warm summer, low-flow conditions with high biological activity ~~.~~(Zhi et al., 2023). In addition, retention processes in soils and aquifers introduce memory effects and time lags that obscure direct cause–effect relationships (Ehrhardt et al., 2021; Van Meter et al., 2016). Furthermore, water-quality observations typically include a wide range of variables grouped into, e.g.~~,~~, physical, chemical, nutrients, pesticides, metals, and biological, that are tightly linked through shared hydrological flow paths and biogeochemical controls. Although individual time series are often sparse and asynchronous, their interdependence implies that they contain substantial structural information about the coupled system. While such process complexity is difficult to represent and ~~parameterize~~parameterise in traditional process-based models, it aligns well with the

strengths of DL, which can learn nonlinear relationships and cross-variable dependencies directly from data. These relationships suggest that jointly ~~modeling~~modelling multiple variables can increase the effective information content of the data. ~~Realizing~~Realising this potential, however, requires models that explicitly account for the distinct environmental drivers of each constituent and the interactions between the variables (Xia et al., 2025).

Taken together, these characteristics suggest that jointly ~~modeling~~modelling hydrological states and water-quality variables may provide a promising path forward (Fohrer et al., 2022). By explicitly linking water quantity and quality within a unified ~~modeling~~modelling framework, it becomes possible to exploit their shared controls and interactions, effectively increasing the information available for learning even under sparse observation conditions. In particular, multi-target approaches that leverage both continuous hydrological signals (e.g~~.~~. discharge) and irregular water-quality observations can help constrain model ~~behavior~~behaviour and improve the representation of coupled processes (Zhang et al., 2016). Such approaches align naturally with DL architectures that are able to learn shared latent representations across variables and scales. As a result, integrating water quantity and quality in a combined ~~modeling~~modelling framework may not only mitigate current data limitations but also enable more consistent and statistically robust predictions of hydro-biogeochemical dynamics (Ouyang et al., 2025; Xia et al., 2025).

A promising, yet still underexplored, extension in this context is self-supervised learning (SSL), which has recently been applied to hydrological variables such as soil moisture and streamflow (Ghosh et al., 2022; Wang et al., 2025) but has not yet been adopted for in-situ riverine WQ ~~modeling~~modelling (potentially due to the scarcity of the observations themselves). Rather than relying exclusively on predefined target variables, SSL leverages the multivariate structure of hydrological data by training models to reconstruct, predict, or contrast partially observed inputs (Liu et al., ~~2021~~2023). In doing so, the model is forced to learn the joint statistical dependencies and temporal dynamics across variables. For instance, reconstructing masked nitrate concentrations from meteorological forcings, discharge, water temperature, and dissolved oxygen requires the model to ~~internalize~~internalise hydro-biogeochemical relationships rather than fitting a single target from predefined input features. This formulation effectively transforms the learning problem into a structured inference task, where missing information must be inferred from the remaining context. As a result, SSL yields representations that are intrinsically compatible with incomplete and irregularly sampled data, as missing values can be handled directly within the training objective through masking rather than requiring explicit imputation, dedicated missing-value embeddings, or additional preprocessing steps. Beyond predictive performance, this makes SSL particularly attractive as a diagnostic tool, enabling the systematic exploration of process-level relationships and hypotheses within complex hydrological systems.

In this study, we first investigate how the performance of an LSTM-based model changes as additional target variables are incorporated into the learning task. Starting from single-target models for discharge and six individual water-quality variables, we progressively increase the level of integration by jointly simulating pairs of variables and, ultimately, the full set of hydrological and water-quality targets within a multi-target framework. This hierarchical setup allows us to assess whether

and how multi-target learning affects predictive skill and the model's ability to exploit cross-variable dependencies and interactions. Building on the best-performing multi-target configuration, we then evaluate the effect of SSL, testing whether SSL-based training strategies can further improve representation learning and downstream predictions, and discussing their advantages and limitations.

2 Data

Our study leverages the Catchment Attributes and MEteorology for Large-Sample Studies in Germany (CAMELS-DE) dataset (Loritz et al., 2024), supplemented by stream water chemistry data from the QUality, DIscharge and Catchment Attributes for large-sample studies in Germany (QUADICA) dataset (Ebeling et al., 2026). We divided the time series into three distinct time periods for training (2000-10-01 to 2010-09-30), validation (1990-10-01 to 1995-09-30~~))~~,, and testing (2010-10-01 to 2019-09-30). Training and testing are the time periods with the highest number of measurements in the dataset. ~~From~~Of the 1386 monitoring stations present in QUADICA, 554 are matched to catchments in the CAMELS-DE dataset (Ebeling et al., 2026). Applying additional data availability criteria, a catchment is kept only if the dataset contains sufficient WQ observations in both the training period and the test period (validation period was only used to identify hyperparameters). Specifically, at least three different WQ variables (NO_3-N, PO_4-P, DO) must each have 10 or more measurements within the training and testing period respectively, ensuring that the basin contains a minimal amount of multivariate water-quality information for both model training and evaluation. The resulting dataset contains 408 catchments distributed over Germany (Fig. 1).

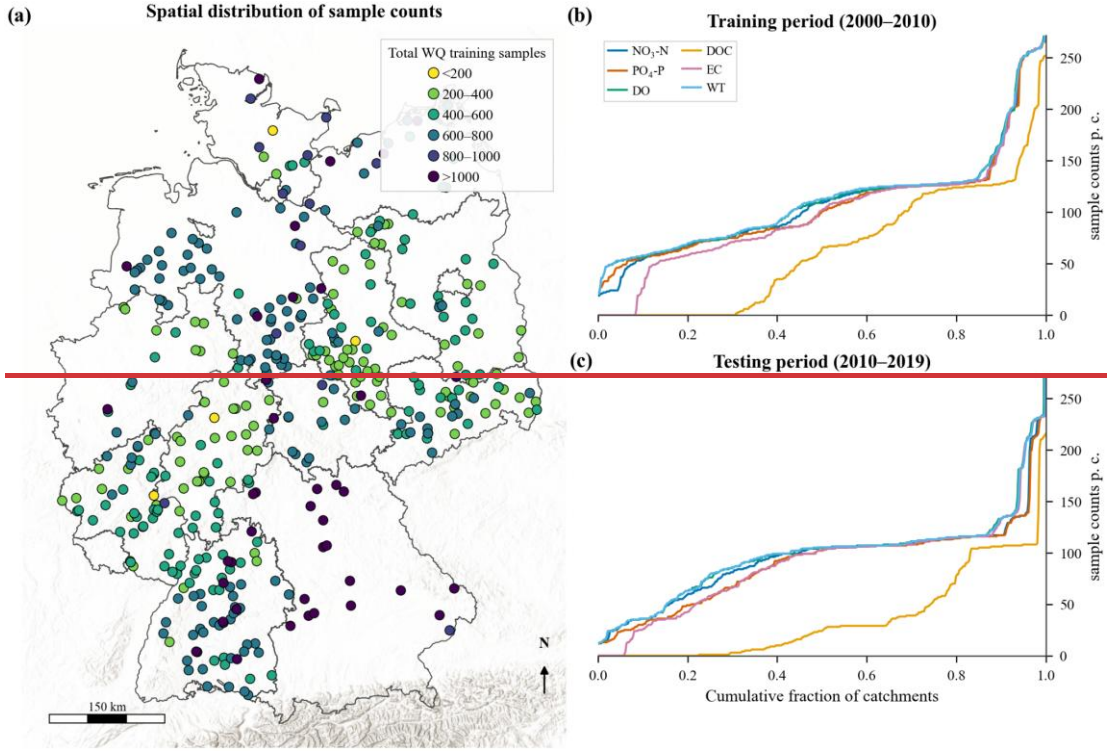
(a)
Spatial distribution of sample counts
Total WQ training samples
<200
200–400
400–600
600–800
800–1000
>1000
N
150 km
(b)
Training period (2000–2010)
NO3-N
PO4-P
DO
DOC
EC
WT
sample counts p. c.
(c)
Testing period (2010–2019)
Cumulative fraction of catchments

111

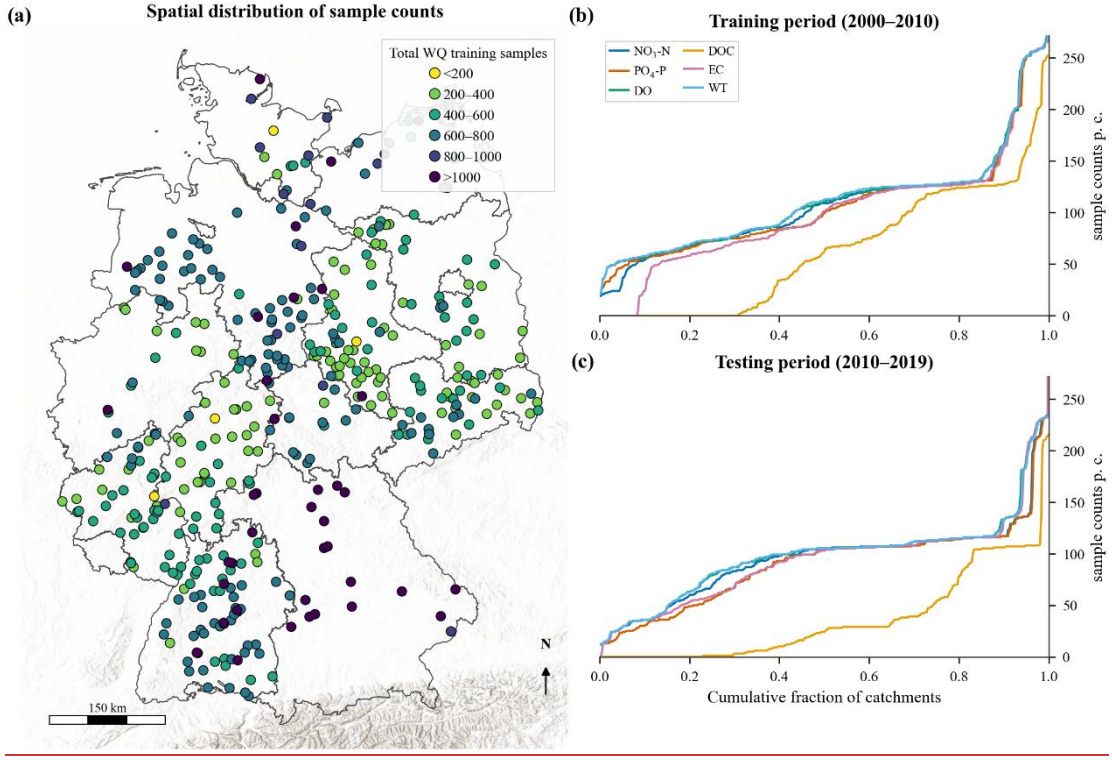
(a)
Spatial distribution of sample counts
Total WQ training samples
<200
200–400
400–600
600–800
800–1000
>1000
N
150 km
(b)
Training period (2000–2010)
NO3-N
PO4-P
DO
DOC
EC
WT
sample counts p. c.
(c)
Testing period (2010–2019)
Cumulative fraction of catchments

112

Figure 1. WQ data availability across the 408 selected CAMELS-DE catchments. **(a)** Spatial distribution of all WQ grab sample counts per ~~gauging station~~catchment (p. c.) during the training period (2000–2010). **(b, c)** Cumulative distribution functions for the sample counts per catchments during the training & testing periods. Appendix C contains further metrics for data distributions. Basemap: Esri World Hillshade (sources: Esri, USGS, NOAA). Federal state boundaries: © GeoBasis-DE / BKG.

2.1 Meteorological forcing, catchment attributes, and streamflow from CAMELS-DE

To simulate streamflow and water-quality dynamics, the models require information on both the temporal evolution of meteorological conditions and the static characteristics of the catchments. Meteorological forcings provide the time-varying drivers of hydrological and biogeochemical processes, while static catchment attributes describe landscape properties that influence how catchments respond to these forcings.

The meteorological forcing used in this study includes daily mean, minimum, and maximum precipitation (P, mm~~)~~ d^{-1}) and temperature (T, °C), as well as global radiation (R, W m^{-2}~~)~~$^{-2}$) and relative humidity (H, %). The data was taken from the CAMELS-DE large sample dataset where HYDrometeorological RASterdata (HYRAS), provided by the Deutscher Wetterdienst (DWD, German Weather Service), was extracted and spatially aggregated to the catchments. The ~~timeseries~~time series are gap-free for both the training and testing periods. For streamflow, we used the specific observed discharge (Q, mm d^{-1}~~)~~$^{-1}$) from CAMELS-DE, which ~~also contains no gaps~~covers 97.3 % (training) and 95.5 % (testing) for the selected ~~period~~periods and catchments. In addition to these dynamic variables, 17 static attributes are provided to all models as time-invariant inputs. These attributes represent differences in catchment topography, soil properties, land cover, and climatic conditions. This set follows the static attributes selected for the baseline model in CAMELS-DE (Loritz et al., 2024).

2.2 Water quality data from QUADICA

We used the grab samples from the QUADICA dataset, containing non-aggregated measurements. From this, we ~~select~~selected six relevant modelled WQ variables including the nutrients nitrate (NO_{3}~~-~~$_{3}$-N, mg L^{-1}) and phosphate (PO_{4}~~-~~$_{4}$-P, mg L^{-1}), dissolved oxygen (DO, mg L^{-1}), dissolved organic carbon (DOC, mg L^{-1}), electrical conductivity (EC, µS cm^{-1}), and water temperature (WT, °C). In contrast to the daily streamflow observations (~~Section~~Sect. 2.1), WQ variables are sparsely sampled. WT and NO_3-N are the most frequently measured variables, with an average temporal coverage of approximately 3 % relative to the continuous streamflow observations (~~Tab.~~Table 1). DOC has the lowest sample count, with 25,~~968~~836 measurements in the training period. The median training sample count for the WQ variables per catchment with samples is between ~~101~~100 and ~~113~~112, except for DOC which has a median sample count of 88. The maximum sample counts per variable within a single catchment generally do not exceed 273~~.~~, except for a few catchments with nearly continuous DO, EC, or WT measurements. The minimum number of training samples per catchment for the variables used in the catchment selection procedure (NO_{3}~~-~~$_{3}$-N, PO_{4}~~-~~$_{4}$-P, and DO) were 19, 21, and 21, respectively, exceeding the threshold of 10 observations imposed during dataset filtering. For most variables, 77–81 % of catchments have a mean sampling interval of 20–50 days, with approximately 10 %

sampled more frequently (10–20 days) and 10 % more sparsely (> 50 days). DOC deviates from this pattern, with fewer catchments in the frequent category (6 %) and more in the sparse category (~~17~~16 %).

Table 1. Number of available WQ samples per variable and sample split period across all catchments. Coverage (%) is calculated relative to the theoretical maximum (408 catchments × number of days in period). For EC and DOC only ~~373~~374 and ~~268~~282 catchments respectively contain sufficient samples during the training period.

Period	NO_3-N	PO_4-P	DO	DOC	EC	WT
Training	44,~~469~~329 (3.0 %)	43,~~700~~572 (2.9 %)	49,~~276~~118 (3.3 %)	25,~~968~~836 (1.7 %)	44,~~295~~152 (3.0 %)	46,~~420~~261 (3.1 %)
Testing	~~39,476~~38,626 (2.9 %)	36,~~637~~752 (2.7 %)	~~43,701~~42,817 (3.~~3~~2 %)	14,~~888~~875 (1.1 %)	~~39,572~~40,855 (3.0 %)	~~40,915~~39,996 (3.~~1~~0 %)

3 Models

In this study, we train ensembles of supervised ($_{\text{baseline}}$LSTM) and self-supervised ($_{\text{self-supervised}}$LSTM) LSTMs on the same training data and compare them on the same testing data. For all model configurations, parameters are ~~optimized~~optimised during training using the mean squared error (MSE) loss. Hyperparameters are selected based on model performance on an independent validation period using the modified Kling–Gupta Efficiency (KGE′; Kling et al., 2012). Final model performance is then evaluated exclusively on the testing period using KGE~~′~~′ (the decompositions of any reported KGE′ values are listed in Appendix B1). To account for uncertainty arising from random parameter ~~initialization~~initialisation, each configuration is trained as an ensemble and ensemble performance is computed as the mean prediction across ensemble members. The ensemble mean is treated as the evaluated model, as it accounts for the stochasticity of weight initialisation and optimisation and outperforms the average single-seed model (Kratzert et al., 2019).

3.1 $_{\text{baseline}}$LSTM configuration, targets, and loss functions

We train an ensemble (N~~=~~ = 5) of ~~regional~~ $_{\text{baseline}}$LSTMs (per configuration) that are commonly applied in rainfall-runoff modelling (e.g. Arsenault et al., 2023; Kratzert et al., 2019) and also increasingly used in WQ modelling (~~e.g.~~ Rahmani et al., 2021; Saha et al., 2023; Zhi et al., 2021, 2024~~, 2021~~). We explored ranges of hyperparameter settings based on previous hydrological studies (Loritz et al., 2024) and found that $_{\text{baseline}}$LSTM performance was relatively stable across a wide range of hyperparameters. We chose hyperparameter settings from Loritz et al. (2024), with modifications made to (a) an increased hidden size (512), (b) an increased number of epochs (50), and (c) the learning rate (~~Tab.~~Table 2). We change the learning rate and number of epochs to make the comparison of training schemes as similar as possible to the $_{\text{self-supervised}}$LSTM (see ~~section~~Sect. 3.2). The remaining hyperparameters are displayed in Table 2.

We consider eight dynamic meteorological features at daily resolution, together with 17 static attributes (see ~~Section~~Sect. 2.1), as input features to the baseline LSTM. As targets, we train different ensemble configurations to assess how model performance is affected by the number of prediction targets and the coupled simulation of WQ and quantity. Specifically, we train ensembles of baseline LSTMs: (i) one ensemble predicting only discharge (Q), (ii) six different ensembles, each jointly predicting discharge and a single WQ variable (Q + NO_3-N, Q + DO, etc.), (iii) six different ensembles taking Q as additional input and each model instance trained on a single WQ variable, (iv) same as (iii) but Q excluded from the input, and (v) two ensembles predicting discharge together with all WQ variables (Q + all WQ). This follows the principle of multi-task learning (Caruana, 1997), where training on related targets can improve ~~generalization~~generalisation through shared representations.

Given this multi-target setup and the strong imbalance in sample coverage between discharge (~~100~~97.3 %) and the WQ variables (1.7–3.3 %), the choice of the loss function becomes critical. We therefore compare two loss formulations: a standard sample-averaged Mean Squared Error (sample-averaged MSE) and a variable-averaged MSE (variable-averaged MSE). The sample-averaged MSE is computed over all available samples in the batch, irrespective of the variable, such that variables with more observations contribute more strongly to the loss. In contrast, the variable-averaged MSE is computed by first calculating the MSE separately for each variable, and then averaging these per-variable errors across variables. This ensures that each variable contributes equally to the batch loss, preventing frequently observed variables (e.g.~~,~~. discharge) from dominating the ~~optimization~~optimisation. A similar issue was addressed in Sadler et al. (2022) via a manually tuned scaling factor on the auxiliary loss. The variable-averaged MSE avoids this additional hyperparameter by averaging per-variable errors directly.

3.2 self-supervised LSTM configuration, targets, and loss functions

Similar to the baseline LSTMs, we train an ensemble (N = 5) of ~~regional~~ self-supervised LSTM models. The overall architecture remains largely unchanged (a single LSTM layer that performs temporal feature extraction, followed by a linear output head that maps hidden states to predictions). However, a key modification is that the six WQ variables, together with Q, are not only treated as prediction targets but, in addition to the eight dynamic meteorological features, are also incorporated as dynamic input features, resulting in a total of 15 dynamic input variables and seven targets. The self-supervised training is based on a masked reconstruction objective inspired by masked autoencoder approaches (e.g.~~,~~ He et al., ~~2021~~2022; Li et al., 2023), adapted here to sparse and irregularly sampled multivariate time series. During training, the model operates on a masking-based reconstruction task. For each training sequence, the seven hydrological and water-quality variables (Q, NO_3-N, PO_4-P, DO, DOC, EC, and WT) are randomly partitioned into two groups. One group is retained as observed input, while the remaining variables are masked by replacing their values with a learned scalar mask token. This token is ~~initialized~~initialised at zero and perturbed with small additive Gaussian noise (scaled by 0.01). The same mask token is also used for missing observations in the input data. Gaps are identified during preprocessing and replaced by the token when the data are passed to the model. This prevents missing values from propagating through the LSTM and allows sequences with incomplete records to be used for training instead of being discarded. In contrast, meteorological forcing variables are always provided as fully

observed inputs and are ~~never~~neither masked nor used as reconstruction targets. ~~The~~ For each training sequence in a batch the number of masked variables ~~per sequence~~ is ~~controlled by a hyperparameter, the masking rate, which is set to 3. This value was determined through hyperparameter tuning~~drawn uniformly between one and ~~means that, for each individual sequence in a batch, exactly three~~seven, and the variables ~~are fully~~to be masked ~~(see also Discussion).~~are then selected at random with equal probability (dynamic masking rate). This way, the training covers the masking configurations of two different inference scenarios which are introduced in the next paragraph. As a result, variables alternate between serving as contextual inputs and reconstruction targets throughout training. This masking strategy enables the model to explicitly leverage cross-variable dependencies. When a subset of variables is observed, it provides contextual information that supports the reconstruction of the masked variables, encouraging the model to learn coherent relationships between water quantity and water-quality dynamics. The dynamic masking rate mimics the different amount of available contextual information during inference. At the same time, this formulation accommodates missing data, as unobserved values can be treated as masked inputs, allowing the model to be trained and applied without requiring explicit imputation or gap-filling. Model training, hyperparameter selection, and evaluation follow the same procedure as for the $_{\text{baseline}}$LSTM models. ~~The~~Apart from the additional dynamic inputs, the only difference is the masking-based learning objective, allowing the impact of the self-supervised formulation to be assessed independently of changes in architecture or training data.

During training, we used a ~~fixed~~dynamic masking rate of ~~three~~one to seven variables per sequence. During evaluation, however, we ~~apply different~~collapse the masking configurations to one or seven masked channels to investigate how well the learned representations can reconstruct variables under varying levels of information availability. We evaluate the $_{\text{self-supervised}}$LSTM under two inference scenarios. In the single-variable masking scenario, all variables except one (Q or a WQ variable) are provided as inputs, and model performance is evaluated on the withheld variable. In the multi-variable masking scenario, only the meteorological forcings and static catchment attributes are provided, while all hydrological and water-quality variables are masked. Model performance is then evaluated separately for each reconstructed target variable.

The single-variable masking scenario assesses the model's ability to exploit cross-variable dependencies when extensive contextual information is available. In contrast, the multi-variable masking scenario represents the most challenging reconstruction setting and mirrors the multi-target prediction setting used for the supervised models, where predictions are generated solely from meteorological forcings and static catchment attributes. Comparing both scenarios therefore provides insight into the extent to which predictive performance originates from information contained in the meteorological forcings versus information shared among hydrological and water-quality variables.

~~The hidden size is increased to 1024, while all remaining hyperparameter settings of the $_{\text{self-supervised}}$LSTM are identical to those of the $_{\text{baseline}}$LSTM configuration (Tab. 2).~~ During training, model parameters are ~~optimized~~optimised using the $_{\text{variable-averaged}}$MSE calculated only over the masked variables.

Table 2. Overview of model architecture, training configuration, and input/output variables. Dynamic inputs were exclusively used as inputs as opposed to the targets which were used as inputs and as targets in the SSL setting.

Category	Parameter	Value
Architecture	Model	LSTM supervised / self-supervised
	Hidden size	512 ~~/ 1024~~
	Dropout	0.3
	Forget gate bias~~Layers~~	3.0
		~~1~~
	Layers	1
Training	Epochs	50
	Batch size	256
	Sequence length	365 d
	Learning rate (scheduled)	~~1e−3 → 5e−4 (ep.~~$10^{-3} \rightarrow 5 \times 10^{-4}$ (epoch 15) → ~~1e−4 (ep.~~10^{-4} (epoch 30) → ~~5e−~~5 ~~(ep.~~$\times 10^{-5}$ (epoch 40)
	Loss function	MSE (sample or variable averaged)
Dynamic inputs (exclusive)	Precipitation (mean, min, max)	mm d^{-1}
	Temperature (mean, min, max)	°C
	Humidity (mean)	%
	Global radiation (mean)	W m^{-2}
Static inputs	Topography	area (km^2), elev_mean (m a.s.l.)
	Soil texture	clay, sand, silt 0–30 cm (%)
	Land cover	artificial, agricultural, forest, wetlands, water (%)
	Climate indices	p_mean, p_seasonality, frac_snow, high/low_prec_freq, high/low_prec_dur
Targets (inclusive)	Specific discharge	mm d^{-1}
	NO_3-N, PO_4-P, DO, DOC	mg L^{-1}
	EC	µS cm^{-1}
	WT	°C

4 Results

~~In section 4.1 we show~~We first present the baselineLSTM and ~~analyze~~analyse how coupled simulations of WQ and ~~quantity~~Q affect overall model performance~~, specifically assessing~~. Specifically, we assess whether multi-task learning leads to improvements or degradations, and how these effects depend on ~~sample~~sampling frequency and the number of available measurements. ~~In section 4.2~~Afterwards we ~~focus on assessing~~assess the self-supervised ~~models, technical challenges~~model. For evaluation, the predictions of all ensemble members are averaged at each time step, and ~~potentials~~this ensemble mean is treated as a single model prediction. Models that use Q as input cannot produce predictions for ~~further work.~~

~~4.1 Coupled water quality~~periods with gaps in the discharge record, even when these gaps are short. All models are therefore evaluated only for the time steps where every model provides a prediction, and ~~quantity simulations using the baseline LSTM~~only in catchments with training observations of that variable. Since reported model differences can be small, and performance metrics are subject to substantial sampling uncertainty (Clark et al., 2021) and can be inflated by counterbalancing errors (Cinkus et al., 2023), we provide an uncertainty quantification for certain model comparisons in Appendix D.

To assess how supervised LSTMs, commonly among the best-performing DL architectures in rainfall–runoff modelling (Liu et al., 2025), respond when predicting multiple targets instead of only streamflow, we evaluate whether their performance declines under multi-task settings or whether they may benefit from shared representations. In this context, all baseline models (~~Section~~Sect. 3.1) achieve high runoff prediction skill, with median ~~KGE'~~KGE′ values between 0.84 and 0.87 (median NSE ∈ [0.87, 0.89]), consistent with previously reported streamflow performance in Germany (Loritz et al., 2024). Extending the model from predicting only discharge to jointly predicting Q and WQ variables leads to only a small decrease in discharge performance (~~ΔKGE'~~ΔKGE′ ≤ 0.03). Overall, this suggests that the baselineLSTM~~baselineLSTM~~ is sufficiently expressive to support multi-target learning without a ~~significant~~notable loss in discharge prediction skill. This is consistent with findings from continuous multi-target settings (Ouyang et al., 2025; Sadler et al., 2022). However, the strong imbalance in temporal coverage between discharge (≈~~100~~97 %) and WQ variables (≈1.7–3.3 %) introduces an additional trade-off, which is primarily governed by the choice of the loss formulation.

The dominant factor influencing WQ predictions in the baselineLSTM is the choice of the loss formulation. Switching from the sample-averagedMSE to the variable-averagedMSE leads to a slight decrease in runoff performance (median KGE′ from 0.87 to 0.84), but ~~consistently~~ improves the prediction of all WQ variables ~~(ΔKGE' ∈ [~~, most pronounced for DOC, NO_3-N, EC, and PO_4-P (ΔKGE′ = 0.~~01, 02~~ 0.~~06~~]), except~~07) and only marginally for DO and ~~PO_4 (ΔKGE'~~WT (ΔKGE′ < 0.01). Henceforth when referencing the multi-target baselineLSTM (Q + 6 WQ), the version that was trained on the variable-averagedMSE loss is meant. ~~Best~~Among the baselineLSTMs, the best performance for ~~all WQ variables, except dissolved oxygen (DO),~~DOC, PO_4-P, EC, and WT is achieved when training the model jointly on discharge and the respective WQ variable as targets (Fig. A1~~). Notably,~~), while for NO_3-N this setup ~~outperforms~~performs on par with the model using discharge as an input (median KGE′ = 0.66

each). Compared to models that include discharge as an input feature ~~together with the meteorological forcing. This suggests that,~~ learning discharge as a co-target ~~helps shape more informative latent representations, which in turn benefits WQ predictions. While the performance gains are modest, they are consistent across all WQ variables (ΔKGE′ ∈ [0.01,~~improves DOC, EC, and PO_4-P (ΔKGE′ = 0.05~~]) except for~~ , 0.04, and 0.03), whereas differences for NO_3-N and WT are negligible (≤ 0.004) and DO ~~(ΔKGE′ < 0.~~is slightly better predicted with discharge as an input (ΔKGE′ = −0.01). In contrast, treating discharge merely as an additional input feature does not yield comparable improvements, with performance remaining largely unchanged (ΔKGE′ < 0.01) relative to models driven only by meteorological forcings, except ~~for minor gains in PO_4-P and EC.~~EC (ΔKGE′ = +0.04).

The predictive performance of the multi-target $_{\text{baseline}}$LSTM (Q + 6 WQ) across the full suite of variables is ~~summarized~~summarised in Fig. 2. While Q and WT are reconstructed with high fidelity, achieving median ~~KGE'~~KGE′ values of 0.84 and 0.~~94~~95, respectively, the accuracy for chemical constituents exhibits substantial variability. The model demonstrates moderate to high skill for DO (median ~~KGE'~~KGE′ = 0.~~71~~74), DOC (median ~~KGE'~~KGE′ = 0.~~62~~66), and NO_3-N (median ~~KGE'~~KGE′ = 0.~~60~~65), whereas PO_4-P remains the most challenging target to reproduce, with a median ~~KGE'~~KGE′ of only 0.~~35~~40. The spatial distribution of these metrics ~~(Fig. 2)~~ reveals distinct regional patterns across the study area~~.~~ (Fig. 2). For NO_3-N (Fig. ~~2a) and DO (Fig.~~2b), ~~the model performs inconsistently across federal states, with notably higher KGE' values observed in northern and eastern Germany. In contrast, the~~ performance ~~for PO_4~~ is highest in northern Germany (median KGE′ of 0.81 to 0.84 in Schleswig-Holstein, Mecklenburg-Western Pomerania, and Lower Saxony) and lowest in Brandenburg, Thuringia, and Hesse (0.44 to 0.49). PO_4-P (Fig. 2c) ~~is markedly lower~~shows the lowest and ~~more~~most heterogeneous~~, characterized by poor predictive skill (KGE'~~ performance, with KGE′ < 0.2~~)~~ in numerous catchments, ~~particularly~~mainly in eastern and central Germany (median KGE′ of 0.14 in Brandenburg, 0.25 in Saxony-Anhalt, and 0.31 in Thuringia). DO (Fig. ~~and southwestern~~2d) is predicted best in the east and south (0.80 to 0.88 in Brandenburg, Saxony, and Bavaria) and lowest in the northwest (0.66 in Schleswig-Holstein and North Rhine-Westphalia). Thus, the regions with low NO_3-N and PO_4-P skill do not coincide with those of low DO skill. However, we could not identify a clear set of catchment or climatic characteristics that consistently explained the observed spatial patterns, suggesting that multiple interacting effects may be involved.

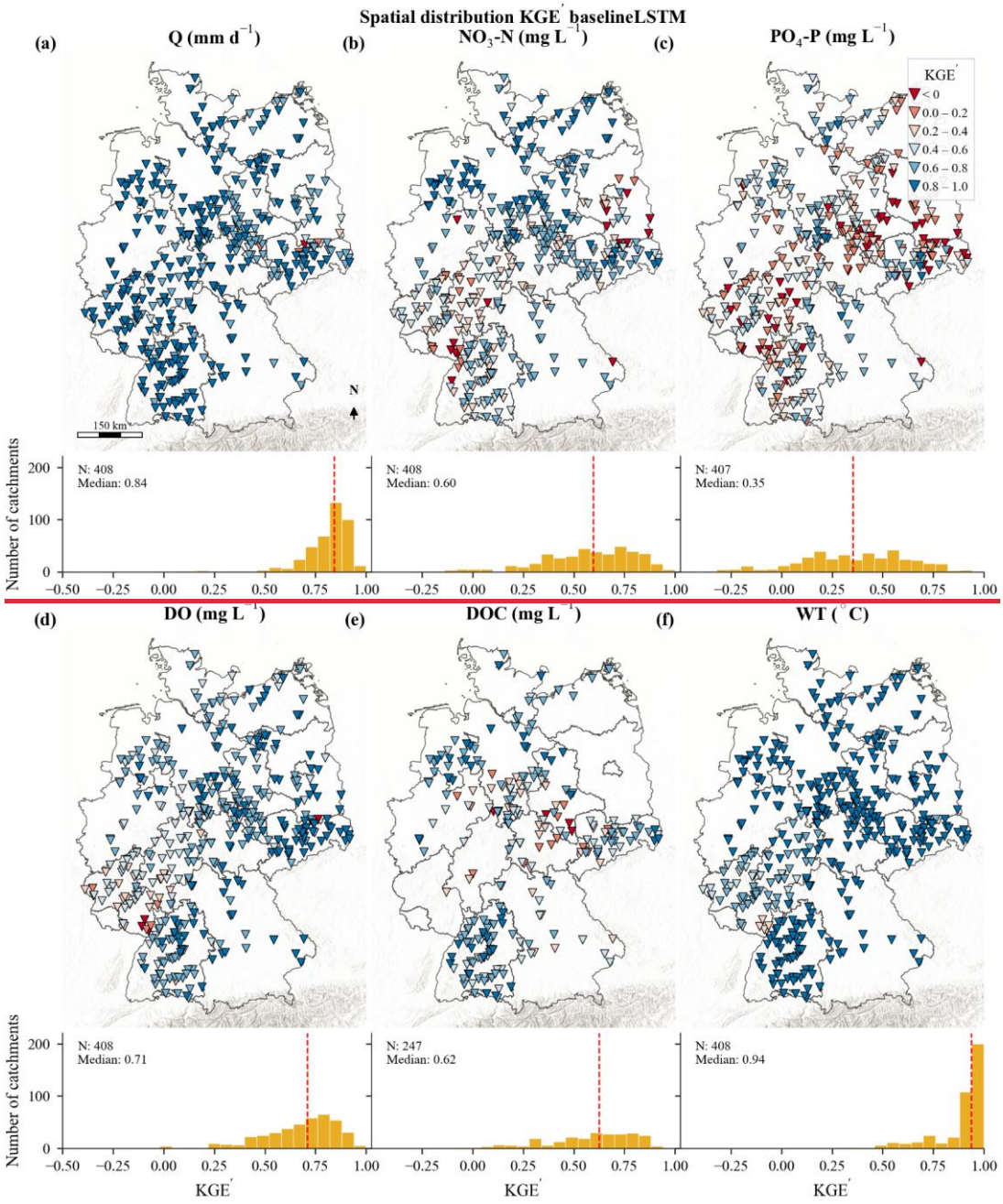
Spatial distribution KGE′ baselineLSTM
(a)
Q (mm d−1)
(b)
NO3-N (mg L−1)
(c)
PO4-P (mg L−1)
KGE′
< 0
0.0 – 0.2
0.2 – 0.4
0.4 – 0.6
0.6 – 0.8
0.8 – 1.0
N
150 km
Number of catchments
N: 408
Median: 0.84
N: 408
Median: 0.60
N: 407
Median: 0.35
(d)
DO (mg L−1)
(e)
DOC (mg L−1)
(f)
WT (°C)
N: 408
Median: 0.71
N: 247
Median: 0.62
N: 408
Median: 0.94
KGE′
KGE′
KGE′

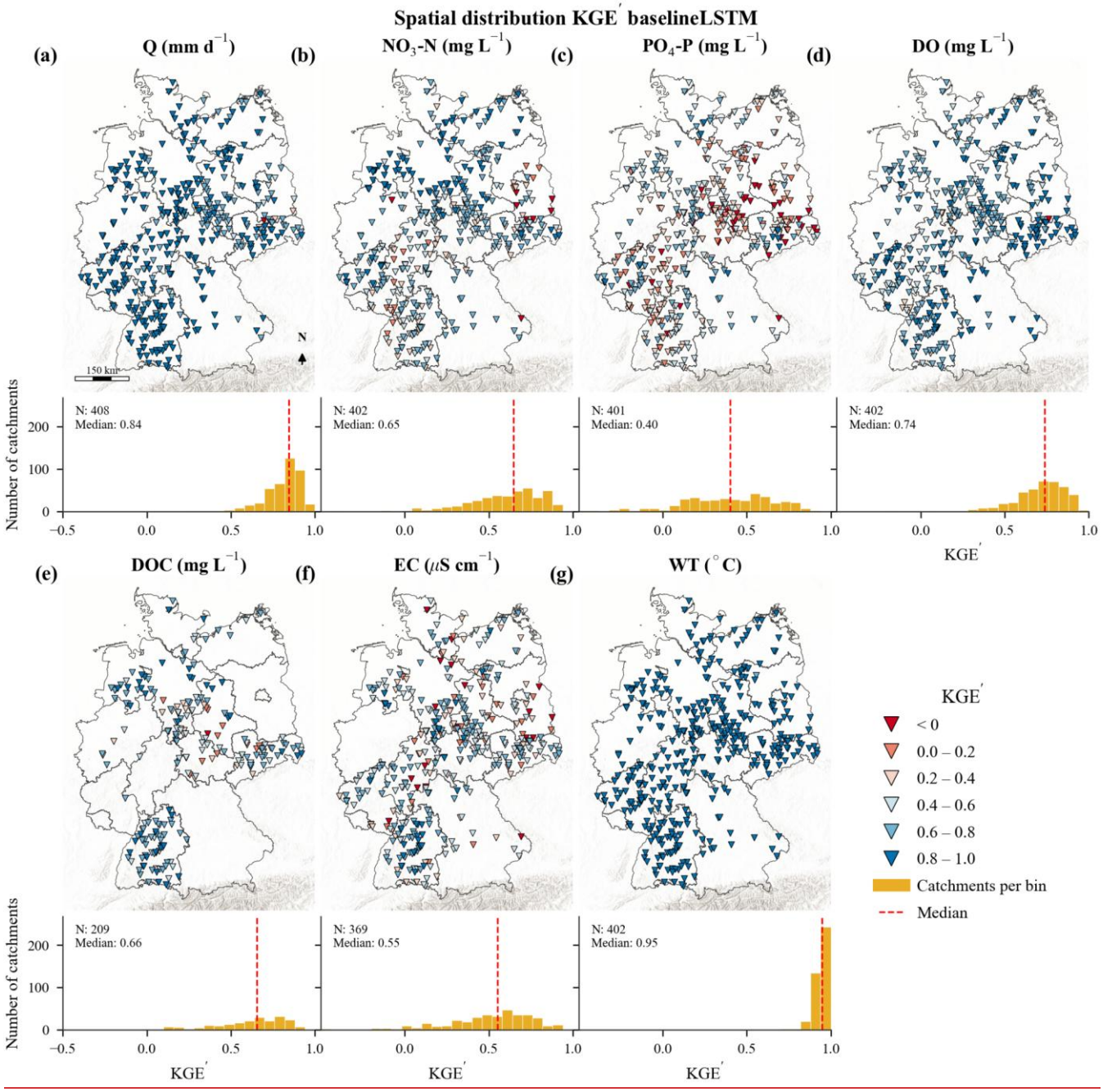

Figure 2. Predictive performance of the multi-target $_{baseline}$LSTM (Q + 6 WQ, variable-averaged loss) on the test period (2010–2019) across ~~408~~all evaluated catchments~~. (.(a eg~~) Spatial distribution of ~~KGE'~~KGE′ for Q, NO_3-N, PO_4-P, DO, DOC, EC, and ~~PO_4-P~~WT. Symbol colour indicates ~~KGE' magnitude~~the KGE′ class according to the legend~~; (d–i) Frequency distributions~~. The histogram below each map shows the frequency distribution of ~~KGE'~~KGE′ across ~~all~~ catchments~~ for Q, NO_3-N, PO_4-P, DO, DOC, and WT. Dashed~~. *N* gives the number of evaluated catchments per variable, and dashed red lines ~~indicate~~mark the median ~~KGE' across all 408 catchments. EC is not shown due to figure layout constraints and is presented separately~~KGE′. Only catchments with WQ

observations of the respective variable in the ~~Appendix~~training period are shown. Basemap: Esri World Hillshade (sources: Esri, USGS, NOAA). Federal state boundaries: © GeoBasis-DE / BKG.

Finally, we examine the relationship between data availability and model performance. As expected for data-driven models, predictive skill generally depends on the amount of available training data; however, this relationship is weak and not consistently expressed across variables. Pearson correlations between the number of samples per catchment and variable and their respective ~~KGE'~~KGE′ values are low (~~ρ <~~$r \leq$ 0.~~31~~34; Cohen, 2013). When considering Spearman rank correlations, only PO_4-P ~~shows~~(ρ = 0.30–0.34) and DOC (ρ = 0.27–0.33) show a moderate relationship ~~(0.36 < ρ < 0.39; Cohen, 2013).~~ This effect becomes more apparent when comparing groups of basins: the median ~~KGE'~~KGE′ for PO_4-P increases substantially (~~ΔKGE'~~ΔKGE′ ∈ [0.~~43;~~37, 0.~~58~~42]) from basins with less frequent sampling (> 50 days, n = 42) to those with average sampling intervals of 10–20 days (n = ~~38) to those with~~36). This relationship is less ~~frequent~~pronounced for the other variables. However, the sampling ~~(≥ 50 days, n = 43). The observed relationships~~ interval groups are ~~not attributable to a strong spatial clustering of highly~~spatially clustered, as sampling frequencies largely follow the monitoring programmes of the federal states: 37 of the 42 catchments with intervals > 50 days are located in Saxony-Anhalt and Saxony, and 17 of the 36 catchments with intervals of 10–20 days in Bavaria. The group difference therefore partly reflects regional differences. Within federal states, more frequently sampled catchments~~, as sampling densities are distributed across the study area.~~ nevertheless show higher PO_4-P performance (e.g. Saxony-Anhalt: median KGE′ = 0.35 for 20–50 days vs 0.14 for > 50 days; Saxony: 0.51 vs 0.36 respectively), indicating that sampling frequency itself contributes. Furthermore, correlations between test-period sample counts and KGE′ are weak (Pearson $r \leq$ 0.13 for all variables except PO_4-P with r = 0.22–0.24; Spearman ρ ~~<~~≤ 0.~~1 for most variables~~18), suggesting that the reported performance patterns are not primarily an ~~artifact~~artefact of differing evaluation sample sizes. Overall, while increased data availability is clearly important for DL applications and can improve performance, it does not uniformly explain model skill, indicating that other factors, such as process complexity in a given catchment and data noise, also play ~~a significant~~an important role (Jeung et al., 2026; Schauer et al., 2025; Xia et al., 2025). ~~This interpretation is supported by a bootstrapping analysis of the test data, in which we resample the observations 1,000 times with replacement and recompute KGE′ for each realization. The resulting performance estimates remain stable across catchments, suggesting that model skill is not overly sensitive to individual observations and extremes.~~

~~4.2 Coupled water quality and quantity simulations using~~For the $_{\text{self-supervised}}$LSTM Under the fully masked inference scenario~~,~~ where ~~both~~ discharge and all WQ variables ~~and discharge~~ are masked during testing, leaving only meteorological forcings and static catchment attributes as input ~~(multi-masking scenario),~~ the $_{\text{self-supervised}}$LSTM achieves performance broadly comparable to the multi-target $_{\text{baseline}}$LSTM ~~(Fig. 3). Most variables show~~, with marginal differences ~~of ≤ 0.01~~ in median ~~KGE'. The most notable deviations are observed~~KGE′ for ~~NO_3-N (ΔKGE' = −0.02) and EC (ΔKGE' = −0.02), indicating a modest tendency for the SSL model to underperform the supervised baseline when no observational context is available at inference time. However, according to a paired bootstrap analysis across catchments, only the reduction in NO_3-N performance is statistically significant.~~

~~Under the single-masking scenario~~all variables ($|\Delta KGE'| \leq 0.014$). Differences are similarly small under the single-masking scenario, where all but one hydrological or water-quality variable are provided ~~to the self-supervised LSTM~~ as contextual information, ~~clear improvements emerge for two variables (Fig. 3). PO_4-P shows the largest gain ($\Delta KGE' = +0.05$), followed by DO (+0.02), while most other variables remain effectively unchanged, with noteworthy improvements in the lower-performing catchment percentiles for DO and WT. A paired bootstrap analysis confirms that the improvements for PO_4-P and DO are statistically significant, whereas~~ although the sign of the differences ~~for the remaining variables are generally not distinguishable from sampling variability. These results suggest that the SSL model is able to exploit cross-variable dependencies when~~varies between variables. Thus, providing contextual ~~information from related variables is available during inference.~~

~~Overall, differences between the SSL and baseline models remain small across both evaluation scenarios, indicating that the~~ observations does not translate into a clear performance advantage over the multi-masking scenario. The self-supervised training strategy therefore does not fundamentally alter predictive performance. ~~Nevertheless, the statistically significant improvements for DO and PO_4-P under the single-masking scenario demonstrate that the SSL model can leverage information shared among hydrological and water-quality variables when such contextual information is available. Conversely, the largely unchanged~~This holds for the hyperparameters adopted from the supervised baselines (Table 2) as well as for the tested variations of hidden size (512, 1024), number of training epochs (50, 100), and masking rate (fixed, dynamic), none of which yielded a consistent performance ~~under the multi-masking scenario suggests that the learned representations do not consistently translate into improved predictions when meteorological forcings constitute the sole source of information.~~

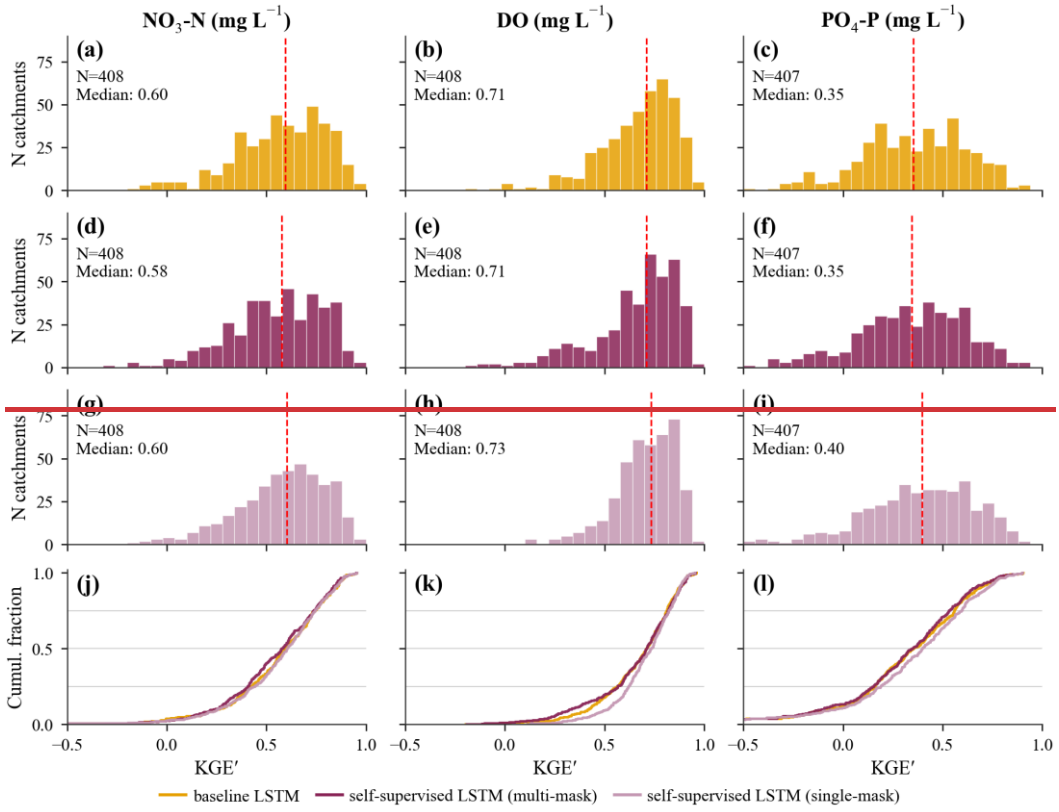

~~**Figure 3.** (a) - (i): KGE' distributions for NO_3-N, DO, and PO_4-P across all catchments for the baseline LSTM (target: Q + 6 WQ variables) and two inference scenarios of~~ advantage for the self-supervised LSTM. Notably, both inference scenarios were evaluated with the same trained ensemble, whereas reproducing them with supervised models would require a separately trained model for each input–output configuration. In addition, unlike the baseline LSTMs that use discharge as input, the self-supervised LSTM~~. The red dotted line denotes the median of the respective populations. The similarity of the distribution underscores the comparability between the two model types. (j)-(l) Empirical cumulative distribution functions (ECDF) of the same three variables. (k) shows how the self-supervised LSTM outperforms the baseline LSTM in the lower percentiles. Appendix B contains ECDFs for all models and variables~~ produces predictions even when input records contain gaps, as missing values are treated as masked inputs.

5 Discussion

The results of this study address two connected questions: 1) whether jointly simulating discharge and multiple water-quality variables in a shared LSTM framework is feasible without compromising predictive skill, and 2) whether SSL can further improve upon this setup. We discuss the first question in ~~section~~Sect. 5.1 and the second question in Sect. 5.2.

It must be mentioned that this study uses the modified ~~KGE'~~KGE′ (Kling et al., 2012), whereas most comparison studies cited below (Liu et al., 2025; Pandit et al., 2025; Xia ~~et al., 2025; Liu~~ et al., 2025) report the original KGE (Gupta et al., 2009). The

newer version of the KGE updates the variability ratio term to avoid covariation with the bias ratio. Even though the differences between those two are mostly negligible, the reported values are not directly interchangeable and should be interpreted accordingly, also since sample set, catchment selection, and periods differ between studies.

5.1 Multi-target learning for coupled water quantity–quality ~~modeling~~modelling

The model results of the $_{\text{baseline}}$LSTM provide several insights into the ~~behavior~~behaviour and potential of multi-target simulation for coupled water quantity–quality ~~modeling~~modelling. First, we find that extending ~~a~~an LSTM network from single-target discharge prediction to a multi-target setting does not necessarily lead to a deterioration in discharge performance. Across all configurations, discharge skill remains in the range of previously reported benchmarks for Germany (Loritz et al., 2024), indicating that the capacity of this comparatively simple DL model, consisting of a single LSTM layer with a linear output head, is sufficient to accommodate additional targets without sacrificing predictive performance. This is a noteworthy advantage over process-based models, where a streamflow performance trade-off during multi-variable calibration can be more pronounced (Wagner et al., 2025) and in line with other studies that investigated the use of DL for predicting WQ and water quantity (e.g. Sadler et al., 2022).

For nitrate, direct benchmarking remains difficult due to differences in data structure, model setup, and study region. Nevertheless, to provide context for the magnitude of the achieved performance, we compare our results to values reported in the literature. Our multi-target $_{\text{baseline}}$LSTM, trained on grab-sample data with approximately 3 % temporal coverage, achieves a median ~~KGE'~~KGE′ of 0.~~60~~65 for NO_3-N, which falls within a similar performance range ~~with~~as the single-target study by Pandit et al. (2025) despite differences in data density (temporal resolution), model configuration, and geographic setting and outperforms the multi-target supervised LSTM model by Xia et al. (2025), which used a comparable number of catchments and temporal resolution. Their reported median KGE values for nutrient-related variables of 0.4 align with our phosphate performance. For dissolved oxygen, Zhi et al. (2021, 2023~~, 2021~~) present LSTM-based models but do not report KGEs. For the 2021 paper they report a median NSE value of 0.53 for their core evaluation group of 84 basins, ~~which resembles~~being slightly lower than our median NSE value for DO of 0.~~55~~59. In their follow up study, Zhi et al. (2023) ~~follow-up paper they~~ improved their ~~models~~model's performance to a median NSE of 0.76 by training it on more basins (580), a longer period (30 years~~)~~), and additional input variables ~~like~~such as biogeochemical conditions, which alone are attributed a ~~+~~0.1 NSE increase~~,~~ ~~and hence~~. These results are therefore not directly comparable with ~~our results~~ours. However, Liu et al. (2025), who reproduce these experiments across 236 catchments from Zhi et al. (2021), report a median KGE of approximately 0.70, again consistent with our findings. Water temperature predictions are also in a similar range to previous studies (NSE ≈ 0.~~96~~98–0.~~98~~99; Rahmani et al., 2021), although we do not observe their reported improvement when including discharge as an input. For phosphate, our performance (~~KGE' <~~KGE′ ≤ 0.~~4~~42) is comparable to Xia et al. (2025). Nevertheless, in contrast to their findings, nitrate shows higher predictive skill in our setup (~~KGE'~~KGE′ ≈ 0.~~60~~61–0.~~62~~66). This overall consistency with the literature suggests that our coupled $_{\text{baseline}}$LSTM, which jointly simulates water quantity and WQ in a multi-target framework,

does not compromise predictive performance but it may ~~rather~~even be advantageous when increasing the number of target variables. This contrasts with process-based water-quality models, where adding calibration targets can introduce parameter trade-offs rather than shared gains. For instance, Molina-Navarro et al. (2017) found that a multi-site, multi-variable water quality calibration achieved the best nutrient-load performance when N and P fractions were considered separately, indicating that fully joint calibration can compromise individual-variable performance. For variables such as DOC or electrical conductivity, broader comparisons remain challenging due to the ~~lack~~scarcity of large-sample benchmarks, although ~~individual studies indicate potentially high~~a continental-scale study indicates moderate predictability ~~under well-observed conditions.~~for conductivity (Xia et al., 2025).

An important step in our modelling study was the shift from a sample-averaged ($_{\text{sample-averaged}}$MSE) to a variable-averaged loss ($_{\text{variable-averaged}}$MSE), which introduces a clear but controlled trade-off: a slight decrease in runoff performance is accompanied by ~~consistent~~ improvements across all water-quality variables, most pronounced for DOC, NO_3-N, EC, and PO_4-P. This trade-off is consistent with the task-weight sensitivity reported by Sadler et al. (2022), who showed that the optimal balance between primary and auxiliary targets is not universal. The $_{\text{variable-averaged}}$MSE provides a simple solution that ensures equal contribution from all targets, though adaptive weighting strategies may offer further refinement. It must be noted though, that through equally weighting those sparsely observed variables, noise and measurement errors present in them will have a greater impact on the training signal. This highlights that properly balancing the contribution of sparsely observed targets is essential in multi-target settings, especially when target variables exhibit large differences in data availability, noise levels, and the complexity of the underlying processes. In this context, learning discharge as a co-target, rather than using it only as an input, emerges as a particularly effective strategy. For ~~most variables (notably~~ DOC, EC, and ~~NO_3-N),~~PO_4-P, jointly predicting discharge improves performance compared to models that either exclude discharge or include it only as an input feature~~.~~ ($\Delta KGE' = 0.03$–0.08). This ~~contrasts with~~extends studies that ~~emphasize~~emphasise the importance of discharge primarily as an input (e.g. Rahmani et al., 2021), and suggests that forcing the model to learn discharge internally leads to more informative latent representations. This is consistent with Sadler et al. (2022), who found that multi-task learning outperforms auxiliary-as-input approaches particularly under sparse observation conditions, potentially reflecting a more consistent internal representation of hydrological states (Lees et al., 2022; Ouyang et al., 2025). ~~Interestingly, this~~ This effect is not observed for ~~dissolved oxygen~~DO, which ~~reflects its stronger dependence~~is predicted slightly better with discharge as an input ($\Delta KGE' = -0.01$), and differences are negligible for WT and NO_3-N (Table D1). For DO and WT this is plausible, since both depend primarily on temperature and ~~biological processes~~energy input rather than direct hydrological forcing (Zhi et al~~.~~, 2023~~) compared to~~), whereas DOC ~~and NO3-N~~ concentrations ~~which~~ are largely hydrologically controlled (Ebeling et al., 2021; ~~Saavedra et al., 2022;~~ Zarnetske et al., 2018). For NO_3-N, the co-target yields only a small per-catchment gain (median $\Delta KGE' = 0.01$) without changing the median performance.

The relationship between data availability and model performance is weaker than might be expected and varies across variables, highlighting the difficulty of water-quality prediction. While increased sampling frequency can improve performance, particularly for PO~~4 P~~$_4$-P, where the effect persists within federal states although sampling frequencies are regionally clustered, the overall correlation between sample count and predictive skill remains low, indicating that data quantity alone does not explain model performance. Instead, factors such as measurement noise, sampling bias, and the intrinsic complexity of the underlying processes play an equally important role (Jeung et al., 2026; Xia et al., 2025). This is reflected in the variable-specific and spatial performance patterns across Germany. While discharge and water temperature are reconstructed with high fidelity, performances for chemical constituents are substantially more variable. In particular, phosphorus remains difficult to predict, both in terms of overall performance and spatial consistency. This suggests that phosphorus dynamics are strongly influenced by local controls, including point sources, legacy effects, and biogeochemical interactions in soils and streams, which operate at finer spatio-temporal scales than those represented by the general catchment attributes and large-scale hydroclimatic drivers used in this study (Ebeling et al., 2021; Gu et al., 2017). Moreover, the absence of explicit nutrient-source information and the 365-day input window limit the model's ability to represent long-term changes in nutrient inputs and legacy effects (Ehrhardt et al., 2021; Westphal et al., 2020), while shorter-term variability resulting from hydrological and seasonal mobilisation processes may be better captured. Future model setups integrating available nutrient source datasets (Batool et al., 2022; Sarrazin et al., 2024) and longer memory or multi-frequency architectures (Acuña Espinoza et al., 2025, 2026) could help address these limitations.

By comparison, NO~~3~~$_3$-N ~~and DOC exhibit~~exhibits a clearer spatial structure, with higher performance in northern Germany. These regions are ~~characterized~~characterised by agricultural lowland catchments with shallow groundwater systems and high hydrological connectivity, where nutrient concentrations are highly dynamic but strongly linked to discharge patterns. Under wet conditions, shallow solute sources become connected to the stream network, whereas deeper flow paths may transport lower solute concentrations due to longer residence times and retention processes such as denitrification (Ebeling et al., 2021). Conversely, catchments with stronger topographic gradients may be affected by a wider range of event-driven and interacting processes with temporally variable source areas and connectivity patterns (Saavedra et al., 2025; Winter et al., 2024), resulting in more heterogeneous and less predictable water-quality responses.

Consistent with this interpretation, we observe higher model performance in catchments with greater internal solute variability, particularly for NO~~3~~$_3$-N ~~and DOC~~, and also for WT. For NO~~3~~$_3$-N, the correlation between ~~KGE'~~KGE′ and the coefficient of variation is ~~approximately~~between 0.~~3~~27 and 0.38 across models and catchments. This indicates that variability itself does not necessarily reduce predictability, provided that it follows structured hydrological controls that can be learned by the model. This relationship is not observed for PO~~4~~$_4$-P, suggesting that phosphorus variability is more strongly governed by processes that are either insufficiently sampled or not well represented by the available predictors. The improved PO~~4~~$_4$-P performance in more densely sampled catchments further supports this interpretation, indicating that low-frequency sampling may fail to

capture the dominant dynamics of phosphorus transport and transformation. This aligns with concepts of spatial and temporal variability in water-quality constituents, which require monitoring strategies adapted to the intrinsic variability of each constituent to capture the relevant processes (Schauer et al., 2025). Relatedly, the "simplicity index" proposed by Xia et al. (2025) shows that model performance strongly correlates with the extent to which a variable's dynamics can be explained by linear relationships with discharge and seasonal cycles. Since during the test period, less than one sample per catchment coincides with discharge above the 99th percentile (0.3 for DOC to 0.9 for DO), the model skill during high-flow events cannot be evaluated with grab-sample data. We therefore did not analyse extreme concentrations, which would require high-frequency or event-based sampling.

5.2 Benefits of self-supervised LSTM training

Regarding the SSL setup, we applied a full-variable masking strategy, i.e., entire hydrological or water-quality variables were masked during training rather than individual time steps or short temporal segments. This choice was motivated by the intended application and the sparse nature of the water-quality observations. During training, ~~three~~one to all of the seven hydrological and water-quality variables are randomly masked, while the remaining variables remain visible. The model is then required to reconstruct the masked variables from the meteorological forcings and the available hydrological and water-quality information. Because the set of masked variables changes from one training sequence to the next, different combinations of variables repeatedly act as contextual inputs and reconstruction targets throughout training. Over time, this encourages the model to learn statistical dependencies among variables, as successful reconstruction requires exploiting information contained in the observed variables~~.~~ (cf. Zerveas et al., 2021). The goal is that the model gradually learns a shared representation of water quantity and water-quality dynamics that can be used to infer missing variables from the available context.

We selected full-variable masking because it aligns naturally with the inference scenarios considered in this study, where complete variables are unavailable and must be reconstructed from the remaining information. We did compare alternative masking strategies, such as masking individual time steps or short temporal segments ~~but~~and found the full-variable masking worked best in our scenario. Although recommended in Li et al. (2023), such approaches may be more appropriate for applications focused on gap-filling or interpolation of partially observed time series. For example, if high-frequency observations of WT and DO are available while NO_3-N, DOC, or PO_4-P are sampled less frequently, temporally ~~localized~~localised masking could be used to learn the reconstruction of missing observations within otherwise observed time series. The number of masked variables per sequence, as well as the selection of which variables are masked jointly, represents an important hyperparameter and defines a continuum between supervised and self-supervised learning. Masking only a small subset of variables moves the training objective closer to a supervised setting, whereas masking a larger number of variables enforces reconstruction from increasingly limited contextual information. ~~The intermediate~~Not masking ~~strategy (no masking of~~ the meteorological variables~~) applied here~~ represents one point in this design space ~~that we found to perform~~. It performed well during hyperparameter tuning and suits both the data set, in which the meteorological forcings are gap-free, and the

inference tasks, in which they are always available. A dynamic masking rate matches the two inference scenarios better than a fixed rate. A more systematic exploration of variable-specific masking rates, training duration, and structured masking strategies, where physically related variables are masked jointly, remains an important direction for future work.

From a technical perspective, SSL simplifies both model development and data handling. A single model can be trained once and subsequently applied across a wide range of input–output configurations without retraining, eliminating the need to build separate supervised models for different target combinations. At the same time, missing values do not require explicit treatment, as masking is an inherent part of the training objective. Consequently, incomplete observations can be incorporated directly into the learning process, avoiding the need for imputation, dedicated missing-value encodings, or additional preprocessing steps (e.g. Gauch et al., 2025). This combination of flexibility and robustness ~~substantially~~ reduces computational cost and streamlines the ~~modeling~~modelling workflow, which is particularly beneficial in hydrological applications ~~characterized~~characterised by heterogeneous and incomplete data.

From a methodological perspective, SSL provides a framework to systematically investigate relationships between variables. By reconstructing selected variables from different subsets of inputs, the model is forced to learn the underlying dependencies within the hydro-biogeochemical system. This enables targeted analyses of how information is shared across variables, for example by assessing how well a given variable can be inferred from others or how predictive skill changes when specific inputs are removed. In this sense, SSL is one way to extend the role of DL models beyond prediction, allowing them to be used as tools to probe and interpret the structure of complex environmental systems.

In this study, the SSL-trained model performs ~~similar~~similarly to its supervised counterpart ~~in terms of benchmark performance,~~ but does not outperform~~. However~~ it. Nevertheless, this comparable skill is achieved with a single trained model that can be applied to different combinations of available inputs without retraining, whereas supervised models must be trained separately for each configuration. Moreover, there is emerging evidence that SSL can improve ~~generalization~~generalisation under unseen conditions (Wang et al., 2025), suggesting that its benefits may become more apparent in spatially out-of-sample scenarios. We therefore argue that SSL should not primarily be viewed as a means to ~~maximize~~maximise predictive skill in conventional benchmarks, but rather as a methodological step ~~toward~~towards more flexible, scalable, and ~~generalizable~~generalisable hydrological models. More broadly, the SSL training paradigm aligns conceptually with emerging foundation models for Earth system prediction, in which a single model trained on diverse data is subsequently adapted to new tasks or variables with minimal retraining and little computational cost (Bodnar et al., 2025; Lehmann et al., ~~2025~~2026). Taken together, these findings indicate that the potential of SSL may not be fully reflected by conventional benchmark metrics and should also be evaluated in terms of robustness, transferability, and the ability to learn from heterogeneous environmental observations.

6 Conclusion

Our results support four main conclusions: ~~i) there is practically no detrimental effect on~~

i) coupling streamflow with various water-quality variables~~, with Q prediction skill remaining within ΔKGE'~~ in a single LSTM comes at virtually no cost to discharge performance ($\Delta KGE' \leq 0.03$ ~~and,~~ $\Delta NSE \leq 0.02$ across all configurations~~. This is further supported by performance levels~~). At the same time, jointly predicting discharge and a water-quality variable gives the highest skill for most water-quality variables compared with models that predict them without discharge, and overall performance is comparable to contemporary studies~~, irrespective of whether discharge is used as an input or as a target.~~.

ii) including streamflow as a target rather than as an input improves performance for DOC, EC, and PO_4-P ($\Delta KGE' = +0.03$ to $+0.05$) and performs on par for NO_3-N and WT, even though observed discharge is not required at inference. Only DO is predicted slightly better with discharge as an input ~~to any other tested WQ variable except DO increases performances.~~($\Delta KGE' = -0.01$). We conjecture this relates to an improved internal hydrological "understanding" of the LSTM, which could be verified by future probing studies. We therefore ~~strongly~~ recommend the ~~usage~~use of streamflow ~~in WQ modelling~~ as an additional target~~,~~ in WQ modelling when using LSTM architectures. This might be extended to other architectures and warrants testing.

iii) unequal coverage between targets must be addressed in the loss formulation during model training. In our study, discharge observations are continuous whereas water-quality measurements are sparse and irregular, creating a strongly unbalanced multi-target setting. Across all tested multi-target LSTM configurations, variable-averaging the per-target MSE consistently improved water-quality predictions at only a minor cost to streamflow performance, providing a simple and hyperparameter-free default for applications with strongly differing observation densities among targets.

iv) SSL ~~modeling~~modelling in hydrology shows no systematic performance benefits over the supervised multi-target baseline under comparable inference conditions (multi-masking), with ~~small reductions for NO_3-N and EC ($\Delta KGE' = -0.02$ each) and otherwise near-identical medians. When the SSL model is given full cross-variable context (single-masking), small median improvements emerge for PO_4-P ($\Delta KGE' = +0.05$) and DO (+0.02), along with robust gains in the lower performance percentiles for DO and WT.~~near-identical performance medians ($|\Delta KGE'| \leq 0.014$). Incorporation of missing data points into the training signal is deemed highly promising, especially for modelling outside of large sample dataset coverage where the meteorological forcings are usually incomplete. Testing for that by noise injection or adding adversarial data to the input data can explore whether SSL makes ~~a~~an LSTM model more robust against uncertainty in the input data. With the additional hyperparameters in SSL only touched on here, there is a ~~huge~~wide variety of exploratory avenues to ~~optimize~~optimise for individual use cases. Overall, multi-target training proves viable, discharge prediction is largely unaffected across all configurations, and targeted adjustments to the loss formulation and target configuration yield consistent improvements in water-quality skill. ~~Self-supervised learning~~SSL, by contrast, offers practical ~~modeling~~modelling flexibility that is particularly relevant given the sparse and heterogeneous nature of water-quality observations without compromising predictive performance. This training paradigm enables the user-friendly incorporation of a vast ~~amount~~number of related variables for

various inference settings with subsets of input data predicting single targets, multiple targets, or simply imputing missing data in a single LSTM model. We believe this is a necessary step forward to attain foundation models that are able to ~~generalize~~generalise not only spatially and over time but also across hydrological subdomains.

Code and data availability

The CAMELS-DE dataset is available at https://doi.org/10.5281/zenodo.13837553 (Loritz et al., 2024). The QUADICA dataset is available at https://doi.org/10.4211/hs.11cd7518f3b74225a5b9e66bfbce362e (Ebeling et al., 2026), while due to data use ~~licenses~~licences raw data cannot be published and are thus deposited in a long-term institutional repository ~~(,~~(https://www.ufz.de/record/dmp/archive/16457, last access: ~~17th of June~~30 October 2026).

Author contributions ~~(CRedit)~~

Jean-Paul Brede: Conceptualization, ~~methodology~~Methodology, Software, Formal analysis, Investigation, Validation, Visualization, Writing ~~–~~– original draft, Writing ~~–~~– review & editing.
Pia Ebeling: Conceptualization, Data curation, Writing ~~–~~– review & editing.
Jens Kiesel: Writing ~~–~~– review & editing.
Ralf Loritz: Conceptualization, Funding acquisition, Methodology, Resources, Supervision, Writing ~~–~~– original draft, Writing ~~–~~– review & editing.

Financial ~~Support~~ support

The results were funded by the Federal Ministry of Research, Technology and Space (BMFTR) as part of the project “AI-based flood prediction in small river basins in Germany” (KI-HopE-De, 16IS24088A). We are grateful to the Volkswagen Foundation for funding the project “Invigorating Hydrological Science and Teaching: Merging Key Legacies with New Concepts and Paradigms” (ViTamins, 0069685).

~~Declaration of competing~~Competing interests

One of the co-authors is a member of the editorial board of Earth System Science Data. The authors declare that they have no other known competing financial interests or personal relationships that could have appeared to influence the work reported in this paper.

Acknowledgements

The authors acknowledge support by the state of Baden-Württemberg through bwHPC. The authors further gratefully acknowledge the computing time provided on the high-performance computer HoreKa by the National High-Performance Computing Center at KIT (NHR@KIT). This ~~center~~centre is jointly supported by the Federal Ministry of Research, Technology and Space and the Ministry of Science, Research and the Arts of Baden-Württemberg, as part of the National High-Performance Computing (NHR) joint funding program. HoreKa is partly funded by the German Research Foundation (DFG). This work is additionally supported by the Helmholtz Association Initiative and Networking Fund on the HAICORE@KIT partition.

AI ~~Usage~~usage

AI tools were used for script generation, code autocomplete, and plausibility checks. Grammar and spelling checks of the manuscript were also supported by AI. Models used for programming-related tasks were Anthropic's Claude (Sonnet and Opus families) for script generation and Microsoft's Copilot for code autocomplete. Natural language-related tasks were model-agnostic.

~~**Review statement**~~

References

Acuña Espinoza, E., Kratzert, F., Klotz, D., Gauch, M., Álvarez Chaves, M., Loritz, R., and Ehret, U., 2024.: Technical note: An approach for handling multiple temporal frequencies with different input dimensions using a single LSTM cell. EGUsphere 1–12., Hydrol. Earth Syst. Sci., 29, 1749–1758, https://doi.org/10.5194/egusphere-2024-3355-hess-29-1749-2025, 2025.

Acuña Espinoza, E., Álvarez Chaves, M., Kratzert, F., Klotz, D., Gauch, M., Lang, R., Elfgang, D., Dolich, A., Loritz, R., and Ehret, U.: Everything everywhere all at once: A single-cell LSTM network unifying multi-frequency, missing data, and discharge assimilation for robust operational flood forecasting, EGUsphere [preprint], https://doi.org/10.5194/egusphere-2026-4885, 2026.

Arsenault, R., Martel, J.-L., Brunet, F., Brissette, F., and Mai, J., 2023.: Continuous streamflow prediction in ungauged basins: long short-term memory neural networks clearly outperform traditional hydrological models., Hydrol. Earth Syst. Sci., 27, 139–157., https://doi.org/10.5194/hess-27-139-2023, 2023.

Batool, M., Sarrazin, F. J., Attinger, S., Basu, N. B., Van Meter, K., and Kumar, R.: Long-term annual soil nitrogen surplus across Europe (1850–2019), Sci. Data, 9, 612, https://doi.org/10.1038/s41597-022-01693-9, 2022.

Bodnar, C., Bruinsma, W. P., Lucic, A., Stanley, M., Allen, A., Brandstetter, J., Garvan, P., Riechert, M., Weyn, J. A., Dong, H., Gupta, J. K., Thambiratnam, K., Archibald, A. T., Wu, C.-C., Heider, E., Welling, M., Turner, R. E., and Perdikaris, P., 2025.: A foundation model for the Earth system., Nature, 641, 1180–1187., https://doi.org/10.1038/s41586-025-09005-y, 2025.

Caruana, R., 1997.: Multitask Learning., Mach. Learn., 28, 41–75., https://doi.org/10.1023/A:1007379606734, 1997.

Cinkus, G., Mazzilli, N., Jourde, H., Wunsch, A., Liesch, T., Ravbar, N., Chen, Z., and Goldscheider, N.: When best is the enemy of good – critical evaluation of performance criteria in hydrological models, Hydrol. Earth Syst. Sci., 27, 2397–2411, https://doi.org/10.5194/hess-27-2397-2023, 2023.

Clark, M. P., Vogel, R. M., Lamontagne, J. R., Mizukami, N., Knoben, W. J. M., Tang, G., Gharari, S., Freer, J. E., Whitfield, P. H., Shook, K. R., and Papalexiou, S. M.: The Abuse of Popular Performance Metrics in Hydrologic Modeling, Water Resour. Res., 57, e2020WR029001, https://doi.org/10.1029/2020WR029001, 2021.

Cohen, J., 2013.: Statistical Power Analysis for the Behavioral Sciences, 2nd ed., Routledge, New York., 567 pp., https://doi.org/10.4324/9780203771587, 2013.

Ebeling, P., Kumar, R., Weber, M., Knoll, L., Fleckenstein, J. H., and Musolff, A.: Archetypes and Controls of Riverine Nutrient Export Across German Catchments, Water Resour. Res., 57, e2020WR028134, https://doi.org/10.1029/2020WR028134, 2021.

Ebeling, P., Hubig, A., Wachholz, A., Scharfenberger, U., Haug, S., Nguyen, T., Sarrazin, F., Batool, M., Musolff, A., and Kumar, R., 2026.: QUADICA v2: extending the large-sample data set for water QUAlity, DIscharge and Catchment Attributes in Germany., Earth Syst. Sci. Data, 18, 691–712, https://doi.org/https://doi.org/10.5194/essd-18-691-2026, 2026.

Ebeling, P., Ehrhardt, S., Ebeling, P., Dupas, R., Kumar, R., Weber, M., Knoll, L., Fleckenstein, J. H., and Musolff, A., 2021. Archetypes and Controls of Riverine Nutrient Export Across German Catchments. Water Resour. Res. 57, e2020WR028134. https://doi.org/10.1029/2020WR028134

.:Ehrhardt, S., Ebeling, P., Dupas, R., Kumar, R., Fleckenstein, J.H., Musolff, A., 2021. Nitrate Transport and Retention in Western European Catchments Are Shaped by Hydroclimate and Subsurface Properties., Water Resour. Res., 57, e2020WR029469, https://doi.org/10.1029/2020WR029469, 2021.

Fohrer, N., Wagner, P. D., Kiesel, J., Haas, M., and Guse, B., 2022.: A guideline for spatio-temporal consistency in water quality modelling in rural areas., Hydrol. Process., 36, e14711., https://doi.org/10.1002/hyp.14711, 2022.

Gauch, M., Kratzert, F., Klotz, D., Nearing, G., Cohen, D., and Gilon, O., 2025.: How to deal w___ missing input data. EGUsphere 1–21., Hydrol. Earth Syst. Sci., 29, 6221–6235, https://doi.org/10.5194/egusphere-hess-29-6221-2025, 2025 1224.

Ghosh, R., Renganathan, A., Tayal, K., Li, X., Khandelwal, A., Jia, X., Duffy, C., NeiberNieber, J., and Kumar, V., 2022.: Robust Inverse Framework using Knowledge-guided Self-Supervised Learning: An application to Hydrology. https://doi.org/10.48550/arXiv.2109.06429, in: Proceedings of the 28th ACM SIGKDD Conference on Knowledge Discovery and Data Mining, 465–474, https://doi.org/10.1145/3534678.3539448, 2022.

Gu, S., Gruau, G., Dupas, R., Rumpel, C., Crème, A., Fovet, O., Gascuel-Odoux, C., Jeanneau, L., Humbert, G., and Petitjean, P., 2017.: Release of dissolved phosphorus from riparian wetlands: Evidence for complex interactions among hydroclimate variability, topography and soil properties., Sci. Total Environ., 598, 421–431., https://doi.org/10.1016/j.scitotenv.2017.04.028, 2017.

Gupta, H. V., Kling, H., Yilmaz, K. K., and Martinez, G. F., 2009.: Decomposition of the mean squared error and NSE performance criteria: Implications for improving hydrological modelling., J. Hydrol., 377, 80–91., https://doi.org/10.1016/j.jhydrol.2009.08.003, 2009.

He, K., Chen, X., Xie, S., Li, Y., Dollár, P., and Girshick, R., 2021.: Masked Autoencoders Are Scalable Vision Learners., in: 2022 IEEE/CVF Conference on Computer Vision and Pattern Recognition (CVPR), 15979–15988, https://doi.org/10.48550/arXiv.2111.06377 1109/CVPR52688.2022.01553, 2022.

Jeung, M., Her, Y., Baek, S.-S., and Yoon, K., 2026.: Sensitivity of hydrological machine learning prediction accuracy to information quantity and quality., Hydrol. Earth Syst. Sci., 30, 1077–1095., https://doi.org/10.5194/hess-30-1077-2026, 2026.

Kling, H., Fuchs, M., and Paulin, M., 2012.: Runoff conditions in the upper Danube basin under an ensemble of climate change scenarios., J. Hydrol., 424–425, 264–277., https://doi.org/10.1016/j.jhydrol.2012.01.011, 2012.

Kratzert, F., Klotz, D., Shalev, G., Klambauer, G., Hochreiter, S., and Nearing, G., 2019.: Towards learning universal, regional, and local hydrological behaviors via machine learning applied to large-sample datasets., Hydrol. Earth Syst. Sci., 23, 5089–5110., https://doi.org/10.5194/hess-23-5089-2019, 2019.

Lees, T., Reece, S., Kratzert, F., Klotz, D., Gauch, M., De Bruijn, J., Kumar Sahu, R., Greve, P., Slater, L., and Dadson, S. J., 2022.: Hydrological concept formation inside long short-term memory (LSTM) networks., Hydrol. Earth Syst. Sci., 26, 3079–3101, https://doi.org/https://doi.org/10.5194/hess-26-3079-2022, 2022.

Lehmann, F., Ozdemir, F., Soja, B., Hoefler, T., Mishra, S., and Schemm, S., 2025. Finetuning.: Fine-Tuning a Weather Foundation Model withWith Lightweight Decoders for Unseen Physical Processes, J. Geophys. Res. Mach. Learn. Comput., 3, e2025JH000837, https://doi.org/10.48550/arXiv.2506.19088 1029/2025JH000837, 2026.

Li, Z., Rao, Z., Pan, L., Wang, P., and Xu, Z., 2023.: Ti-MAE: Self-Supervised Masked Time Series Autoencoders., arXiv [preprint], https://doi.org/10.48550/arXiv.2301.08871, 2023.

Liu, J., Shen, C., O'Donncha, F., Song, Y., Zhi, W., Beck, H. E., Bindas, T., Kraabel, N., and Lawson, K., 2025.: From RNNs to Transformers: benchmarking deep learning architectures for hydrologic prediction., Hydrol. Earth Syst. Sci., 29, 6811–6828., https://doi.org/10.5194/hess-29-6811-2025, 2025.

Liu, X., Zhang, F., Hou, Z., Wang, Z., Mian, L., Zhang, J., and Tang, J., 2021.: Self-supervised Learning: Generative or Contrastive., IEEE Trans. Knowl. Data Eng. 1–1., 35, 857–876, https://doi.org/10.1109/TKDE.2021.3090866, 2023.

Loritz, R., Dolich, A., Acuña Espinoza, E., Ebeling, P., Guse, B., Götte, J., Hassler, S. K., Hauffe, C., Heidbüchel, I., Kiesel, J., Mälicke, M., Müller-Thomy, H., Stölzle, M., and Tarasova, L., 2024.: CAMELS-DE: hydro-meteorological time series and attributes for 1582 catchments in Germany., Earth Syst. Sci. Data, 16, 5625–5642., https://doi.org/10.5194/essd-16-5625-2024, 2024.

McClain, M. E., Boyer, E. W., Dent, C. L., Gergel, S. E., Grimm, N. B., Groffman, P. M., Hart, S. C., Harvey, J. W., Johnston, C. A., Mayorga, E., McDowell, W. H., and Pinay, G., 2003.: Biogeochemical Hot Spots and Hot Moments at the Interface of Terrestrial and Aquatic Ecosystems., Ecosystems, 6, 301–312., https://doi.org/10.1007/s10021-003-0161-9, 2003.

Minaudo, C., Dupas, R., Gascuel-Odoux, C., Roubeix, V., Danis, P.-A., and Moatar, F., 2019.: Seasonal and event-based concentration-discharge relationships to identify catchment controls on nutrient export regimes., Adv. Water Resour., 131, 103379., https://doi.org/10.1016/j.advwatres.2019.103379, 2019.

Molina-Navarro, E., Andersen, H. E., Nielsen, A., Thodsen, H., and Trolle, D., 2017.: The impact of the objective function in multi-site and multi-variable calibration of the SWAT model., Environ. Model. Softw., 93, 255–267., https://doi.org/10.1016/j.envsoft.2017.03.018, 2017.

Musolff, A., Schmidt, C., Selle, B., and Fleckenstein, J. H., 2015.: Catchment controls on solute export., Adv. Water Resour., 86, 133–146., https://doi.org/10.1016/j.advwatres.2015.09.026, 2015.

Musolff, A., Selle, B., Büttner, O., Opitz, M., and Tittel, J., 2017.: Unexpected release of phosphate and organic carbon to streams linked to declining nitrogen depositions., Glob. Change Biol., 23, 1891–1901., https://doi.org/10.1111/gcb.13498, 2017.

Nearing, G., Cohen, D., Dube, V., Gauch, M., Gilon, O., Harrigan, S., Hassidim, A., Klotz, D., Kratzert, F., Metzger, A., Nevo, S., Pappenberger, F., Prudhomme, C., Shalev, G., Shenzis, S., Tekalign, T. Y., Weitzner, D., and Matias, Y., 2024.: Global prediction of extreme floods in ungauged watersheds., Nature, 627, 559–563., https://doi.org/10.1038/s41586-024-07145-1, 2024.

Ouyang, W., Gu, X., Ye, L., Liu, X., and Zhang, C., 2025.: Exploring Hydrological Variable Interconnections and Enhancing Predictions for Data-Limited Basins Through Multi-Task Learning., Water Resour. Res., 61, e2023WR036593., https://doi.org/10.1029/2023WR036593, 2025.

Pandit, A., Golden, H. E., Christensen, J. R., Lane, C. R., and Husic, A., 2025.: Deep Learning Prediction and Interpretation of Riverine Nitrate Export Across the Mississippi River Basin., Water Resour. Res., 61, e2024WR039207., https://doi.org/10.1029/2024WR039207, 2025.

Rahmani, F., Shen, C., Oliver, S.K., Lawson, K., Ouyang, W., Appling, A., Oliver, S., and Shen, C.: Exploring the exceptional performance of a deepP.,2021. Deep learning approaches for improving prediction of daily stream temperature inmodel and the value of streamflow data scarce, unmonitored, and dammed basins. Hydrol. Process. 35, e14400., Environ. Res. Lett., 16, 024025, https://doi.org/10.1002/hyp.14400 1088/1748-9326/abd501, 2021.

Rathjens, H., Miguez, M. B., Winchell, M., and Sur, R., 2023.: Evaluation of SEAWAVE–QEX in a high agricultural intensity catchment in Belgium., Integr. Environ. Assess. Manag., 19, 513–526., https://doi.org/10.1002/ieam.4688, 2023.

Saavedra, F., Vergopolan, N., Musolff, A., Merz, R., Wang, Z., Winter, C., and Tarasova, L., 2025.: From Soil Moisture Spatial Patterns to Catchment Nitrate Dynamics Using Explainable AI., Water Resour. Res., 61, e2025WR040295., https://doi.org/10.1029/2025WR040295, 2025.

Saavedra, F.A., Musolff, A., von Freyberg, J., Merz, R., Basso, S., Tarasova, L., 2022. Disentangling scatter in long-term concentration–discharge relationships: the role of event types. https://doi.org/https://doi.org/10.5194/hess-26-6227-2022

Sadler, J. M., Appling, A. P., Read, J. S., Oliver, S. K., Jia, X., Zwart, J. A., and Kumar, V., 2022.: Multi-Task Deep Learning of Daily Streamflow and Water Temperature., Water Resour. Res., 58, e2021WR030138, https://doi.org/10.1029/2021WR030138, 2022.

Saha, G. K., Rahmani, F., Shen, C., Li, L., and Cibin, R., 2023.: A deep learning-based novel approach to generate continuous daily stream nitrate concentration for nitrate data-sparse watersheds., Sci. Total Environ., 878, 162930., https://doi.org/10.1016/j.scitotenv.2023.162930, 2023.

Sarrazin, F. J., Attinger, S., and Kumar, R.: Gridded dataset of nitrogen and phosphorus point sources from wastewater in Germany (1950–2019), Earth Syst. Sci. Data, 16, 4673–4708, https://doi.org/10.5194/essd-16-4673-2024, 2024.

Schauer, L. S., Jawitz, J. W., Cohen, M. J., and Musolff, A., 2025.: Spatial and Temporal Variability of River Water Quality., Hydrol. Process., 39, e70154., https://doi.org/10.1002/hyp.70154, 2025.

Van Meter, K. J., Basu, N. B., Veenstra, J. J., and Burras, C. L., 2016.: The nitrogen legacy: emerging evidence of nitrogen accumulation in anthropogenic landscapes., Environ. Res. Lett., 11, 035014., https://doi.org/10.1088/1748-9326/11/3/035014, 2016.

Vaughan, M. C. H., Bowden, W. B., Shanley, J. B., Vermilyea, A., Sleeper, R., Gold, A. J., Pradhanang, S. M., Inamdar, S. P., Levia, D. F., Andres, A. S., Birgand, F., and Schroth, A. W., 2017.: High-frequency dissolved organic carbon and nitrate measurements reveal differences in storm hysteresis and loading in relation to land cover and seasonality., Water Resour. Res., 53, 5345–5363., https://doi.org/10.1002/2017WR020491, 2017.

Wagner, P. D., Duethmann, D., Kiesel, J., Pool, S., Hrachowitz, M., Ceola, S., Herzog, A., Houska, T., Loritz, R., Spieler, D., Staudinger, M., Tarasova, L., Thober, S., Fohrer, N., Tetzlaff, D., Wagener, T., and Guse, B., 2025.: The Unexploited Treasures of Hydrological Observations Beyond Streamflow for Catchment Modeling., WIREs Water, 12, e70018., https://doi.org/10.1002/wat2.70018, 2025.

Wang, L., Shi, L., Reimers, C., Wang, Yanling,Y., He, L., Wang, Yujie,Y., Reichstein, M., and Jiang, S., 2025.: A self-supervised deep learning model for enhanced generalization in soil moisture prediction., J. Hydrol., 662, 133974., https://doi.org/10.1016/j.jhydrol.2025.133974, 2025.

Westphal, K., Musolff, A., Graeber, D., and Borchardt, D.: Controls of point and diffuse sources lowered riverine nutrient concentrations asynchronously, thereby warping molar N:P ratios, Environ. Res. Lett., 15, 104009, https://doi.org/10.1088/1748-9326/ab98b6, 2020.

Winter, C., Jawitz, J. W., Ebeling, P., Cohen, M. J., and Musolff, A., 2024.: Divergence Between Long-Term and Event-Scale Nitrate Export Patterns., Geophys. Res. Lett., 51, e2024GL108437., https://doi.org/10.1029/2024GL108437, 2024.

Xia, X., Liu, X., Liu, J., Fang, K., Lu, L., Oymak, S., Currie, W. S., and Liu, T., 2025.: Identifying trustworthiness challenges in deep learning models for continental-scale water quality prediction., Nexus, 2, 100104., https://doi.org/10.1016/j.ynexs.2025.100104, 2025.

Zarnetske, J. P., Bouda, M., Abbott, B. W., Saiers, J., and Raymond, P. A., 2018.: Generality of Hydrologic Transport Limitation of Watershed Organic Carbon Flux Across Ecoregions of the United States., Geophys. Res. Lett., 45, 11,702–11,711.11702–11711, https://doi.org/10.1029/2018GL080005, 2018.

Zhang, S., Yang,Zerveas, G., Jayaraman, S., Patel, D., Bhamidipaty, A., and Eickhoff, C.: A Transformer-based Framework for Multivariate Time Series Representation Learning, in: Proceedings of the 27th ACM SIGKDD Conference on Knowledge Discovery & Data Mining, 2114–2124, https://doi.org/10.1145/3447548.3467401, 2021.

Zhang, Y., Shao, Q., and Taylor, J. A.: A balanced calibration of water quantity and quality by multi-objective optimization for integrated water system model, J. Hydrol., 538, 802–816, https://doi.org/10.1016/j.jhydrol.2016.05.001, 2016.

H., Yang, D., Jayawardena, A.W., 2016. Quantifying the effect of vegetation change on the regional water balance within the Budyko framework. Geophys. Res. Lett. 43, 1140–1148. https://doi.org/https://doi.org/10.1002/2015GL066952

Zhi, W., Appling, A.P., Golden, H.E., Podgorski, J., Li, L., 2024. Deep learning for water quality. Nat. Water 2, 228–241. https://doi.org/10.1038/s44221-024-00202-z

Zhi, W., Feng, D., Tsai, W.-P., Sterle, G., Harpold, A., Shen, C., and Li, L., 2021.: From Hydrometeorology to River Water Quality: Can a Deep Learning Model Predict Dissolved Oxygen at the Continental Scale??, Environ. Sci. Technol., 55, 2357–2368., https://doi.org/10.1021/acs.est.0c06783, 2021.

Zhi, W., Ouyang, W., Shen, C., and Li, L., 2023.: Temperature outweighs light and flow as the predominant driver of dissolved oxygen in US rivers., Nat. Water, 1, 249–260., https://doi.org/10.1038/s44221-023-00038-z, 2023.

Zhi, W., Appling, A. P., Golden, H. E., Podgorski, J., and Li, L.: Deep learning for water quality, Nat. Water, 2, 228–241, https://doi.org/10.1038/s44221-024-00202-z, 2024.

Appendix A: Complete model performance overview

Appendix A includes tabular overviews over the different model types and the median ~~KGE'~~KGE′ and NSE performances of all models (ensemble mean~~).~~), evaluated for each variable on the same days and catchments for all models (catchments with training observations of the variable; days on which all models provide a prediction). The ~~color~~colour coding presented in Table A1 is applied to all figures.

Table A1. Model configurations shown in Figs. A1–A2. The ~~colored~~coloured square on the left of each heatmap row indicates the model family~~. Empty cells (—) indicate that a variable was not a training target for that configuration.~~

~~Color~~Colour	Model type	Inputs	Target(s)	Variants
	baselineLSTM multi-target	meteorological (8)	Q + 6 WQ	2 (sample-avg. / variable-avg.)
	baselineLSTM paired	meteorological (8)	Q + 1 WQ	6 (one per WQ variable)
	baselineLSTM single-target	meteorological (8)	1 WQ	7 (Q, NO_3-N, DOC, DO, PO_4-P, EC, WT)
	baselineLSTM single-target (+ Q in)	meteorological + Q (9)	1 WQ	6 (NO_3-N, DOC, DO, PO_4-P, EC, WT)
	self-supervisedLSTM	meteorological (~~8~~+ Q + 6 WQ (15)	Q + 6 WQ	1 [8 different inference scenarios: single-mask(7) / multi-mask(1)]

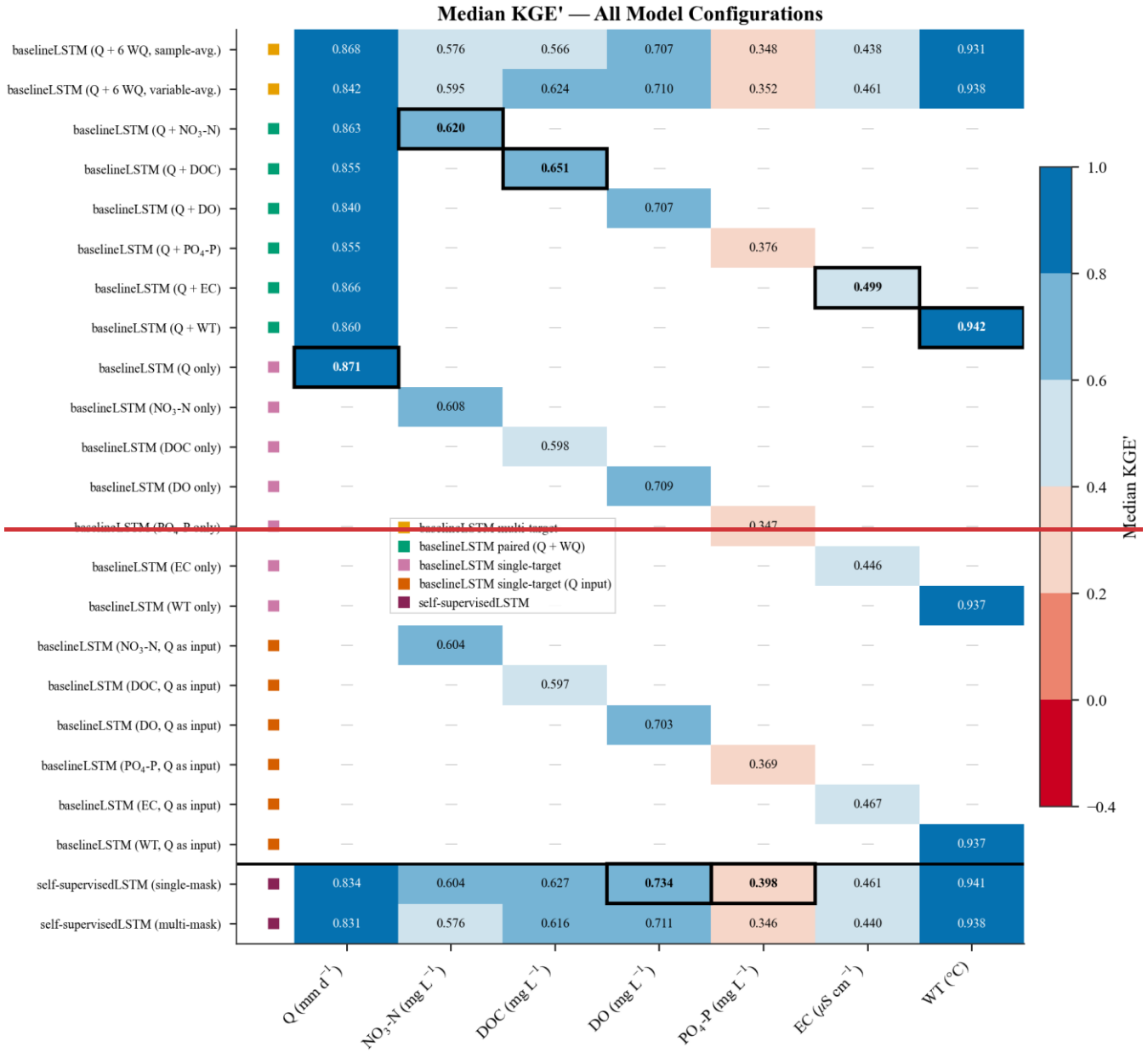
Median KGE' — All Model Configurations
baselineLSTM (Q + 6 WQ, sample-avg.) 0.868 0.576 0.566 0.707 0.348 0.438 0.931
baselineLSTM (Q + 6 WQ, variable-avg.) 0.842 0.595 0.624 0.710 0.352 0.461 0.938
baselineLSTM (Q + NO3-N) 0.863 0.620
baselineLSTM (Q + DOC) 0.855 0.651
baselineLSTM (Q + DO) 0.840 0.707
baselineLSTM (Q + PO4-P) 0.855 0.376
baselineLSTM (Q + EC) 0.866 0.499
baselineLSTM (Q + WT) 0.860 0.942
baselineLSTM (Q only) 0.871
baselineLSTM (NO3-N only) 0.608
baselineLSTM (DOC only) 0.598
baselineLSTM (DO only) 0.709
baselineLSTM (PO4-P only) 0.347
baselineLSTM (EC only) 0.446
baselineLSTM (WT only) 0.937
baselineLSTM (NO3-N, Q as input) 0.604
baselineLSTM (DOC, Q as input) 0.597
baselineLSTM (DO, Q as input) 0.703
baselineLSTM (PO4-P, Q as input) 0.369
baselineLSTM (EC, Q as input) 0.467
baselineLSTM (WT, Q as input) 0.937
self-supervisedLSTM (single-mask) 0.834 0.604 0.627 0.734 0.398 0.461 0.941
self-supervisedLSTM (multi-mask) 0.831 0.576 0.616 0.711 0.346 0.440 0.938
baselineLSTM multi-target
baselineLSTM paired (Q + WQ)
baselineLSTM single-target
baselineLSTM single-target (Q input)
self-supervisedLSTM
Q (mm d−1)
NO3-N (mg L−1)
DOC (mg L−1)
DO (mg L−1)
PO4-P (mg L−1)
EC (µS cm−1)
WT (°C)
Median KGE'
1.0
0.8
0.6
0.4
0.2
0.0
−0.4

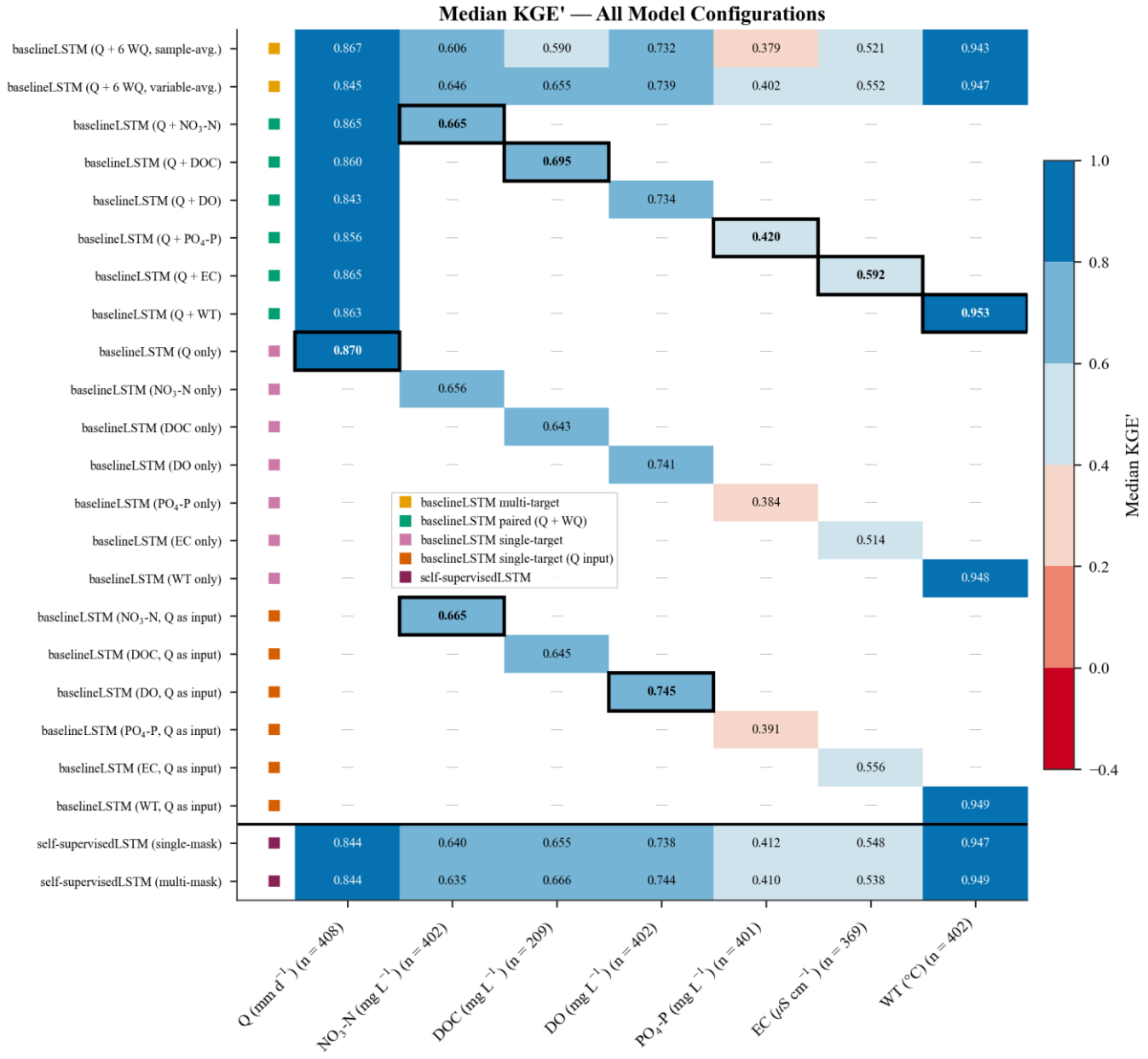

Figure A1. Median KGE′ on the test period (2010–2019) for all model configurations and target variables. Each row corresponds to one model configuration; columns represent the seven target variables. Bold values with a black border mark the best-performing configuration per variable. ~~Dashes~~, *n* gives the number of evaluated catchments per variable dashes (—) indicate that the variable was not a training target for that configuration. ~~Colored~~Coloured squares on the left y-axis indicate the model family (see Table A1).

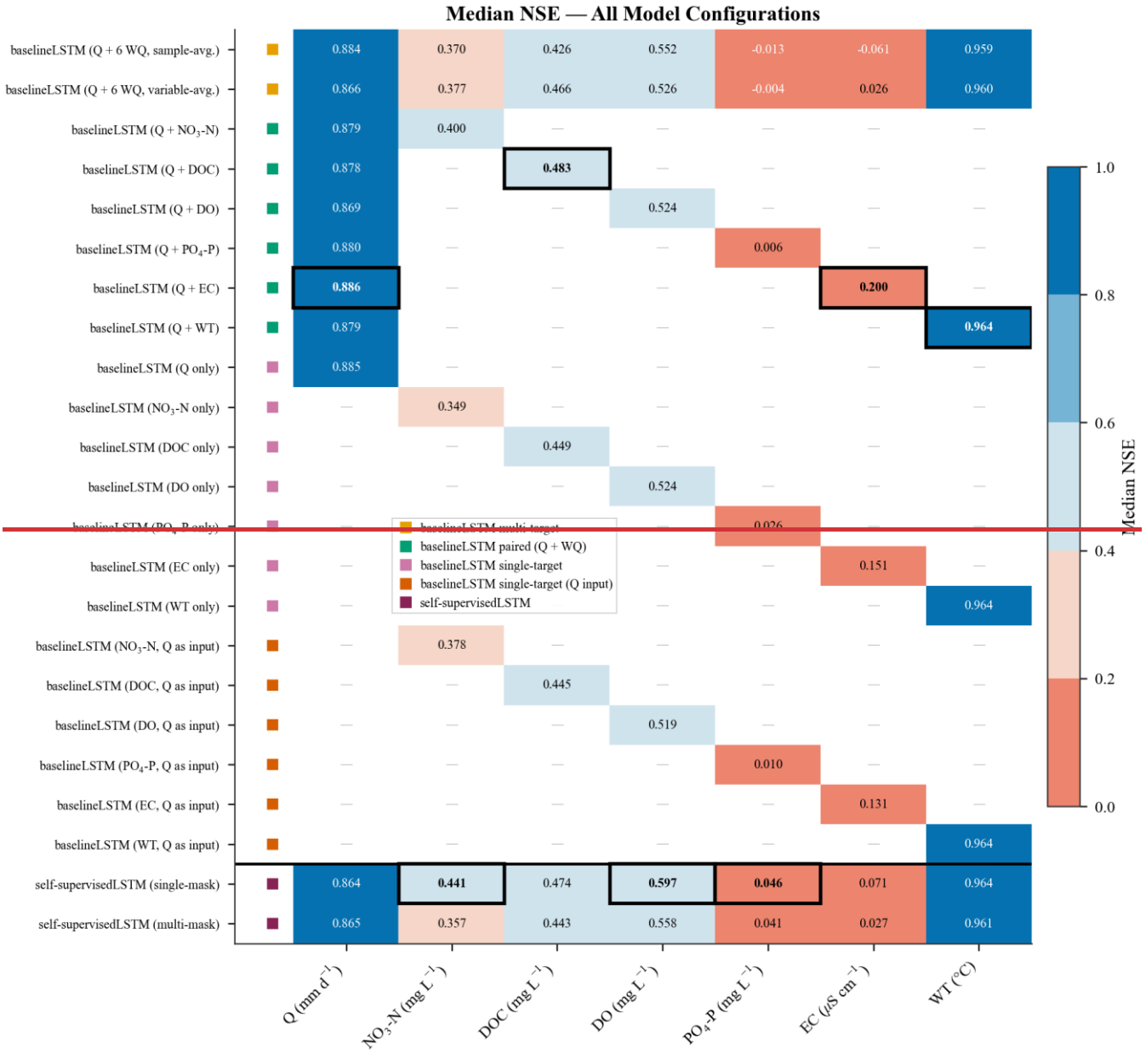
Median NSE — All Model Configurations
baselineLSTM (Q + 6 WQ, sample-avg.)
baselineLSTM (Q + 6 WQ, variable-avg.)
baselineLSTM (Q + NO3-N)
baselineLSTM (Q + DOC)
baselineLSTM (Q + DO)
baselineLSTM (Q + PO4-P)
baselineLSTM (Q + EC)
baselineLSTM (Q + WT)
baselineLSTM (Q only)
baselineLSTM (NO3-N only)
baselineLSTM (DOC only)
baselineLSTM (DO only)
baselineLSTM (PO4-P only)
baselineLSTM (EC only)
baselineLSTM (WT only)
baselineLSTM (NO3-N, Q as input)
baselineLSTM (DOC, Q as input)
baselineLSTM (DO, Q as input)
baselineLSTM (PO4-P, Q as input)
baselineLSTM (EC, Q as input)
baselineLSTM (WT, Q as input)
self-supervisedLSTM (single-mask)
self-supervisedLSTM (multi-mask)
0.884 0.370 0.426 0.552 -0.013 -0.061 0.959
0.866 0.377 0.466 0.526 -0.004 0.026 0.960
0.879 0.400
0.878 0.483
0.869 0.524
0.880 0.006
0.886 0.200
0.879 0.964
0.885
0.349
0.449
0.524
0.026
0.151
0.964
0.378
0.445
0.519
0.010
0.131
0.964
0.864 0.441 0.474 0.597 0.046 0.071 0.964
0.865 0.357 0.443 0.558 0.041 0.027 0.961
baselineLSTM multi-target
baselineLSTM paired (Q + WQ)
baselineLSTM single-target
baselineLSTM single-target (Q input)
self-supervisedLSTM
Q (mm d−1)
NO3-N (mg L−1)
DOC (mg L−1)
DO (mg L−1)
PO4-P (mg L−1)
EC (µS cm−1)
WT (°C)
Median NSE
1.0
0.8
0.6
0.4
0.2
0.0

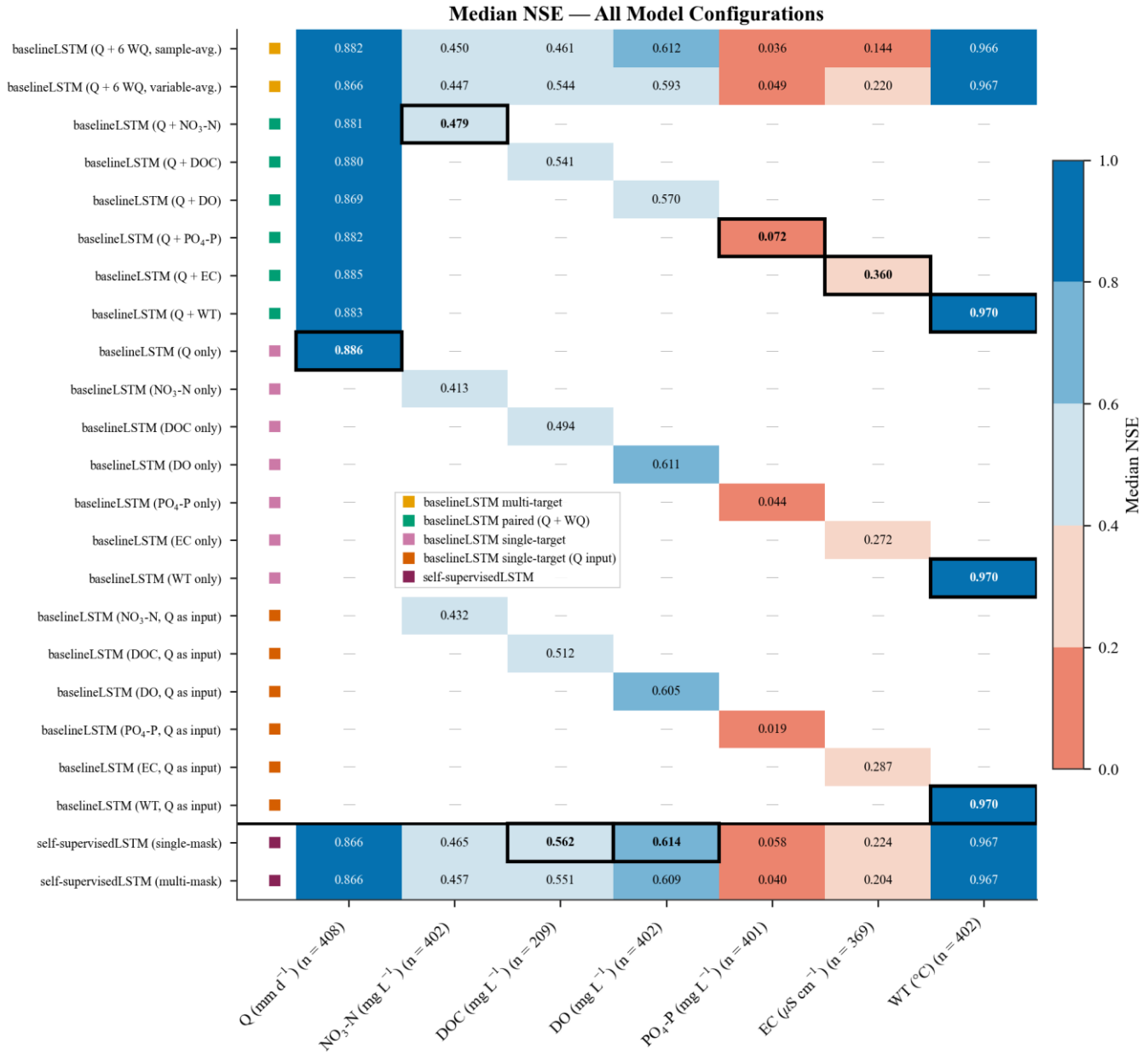

Figure A2. As Fig. A1, but showing median NSE. ~~Shows~~The figure illustrates how a different metric can shift the ~~analysis completely.~~

784 performance rankings (e.g. DOC, DO).

Appendix B: Performance distributions

Appendix B covers ~~KGE'~~KGE′ and NSE performance distribution for all models~~.~~ and an overview of the KGE′ components for all models.

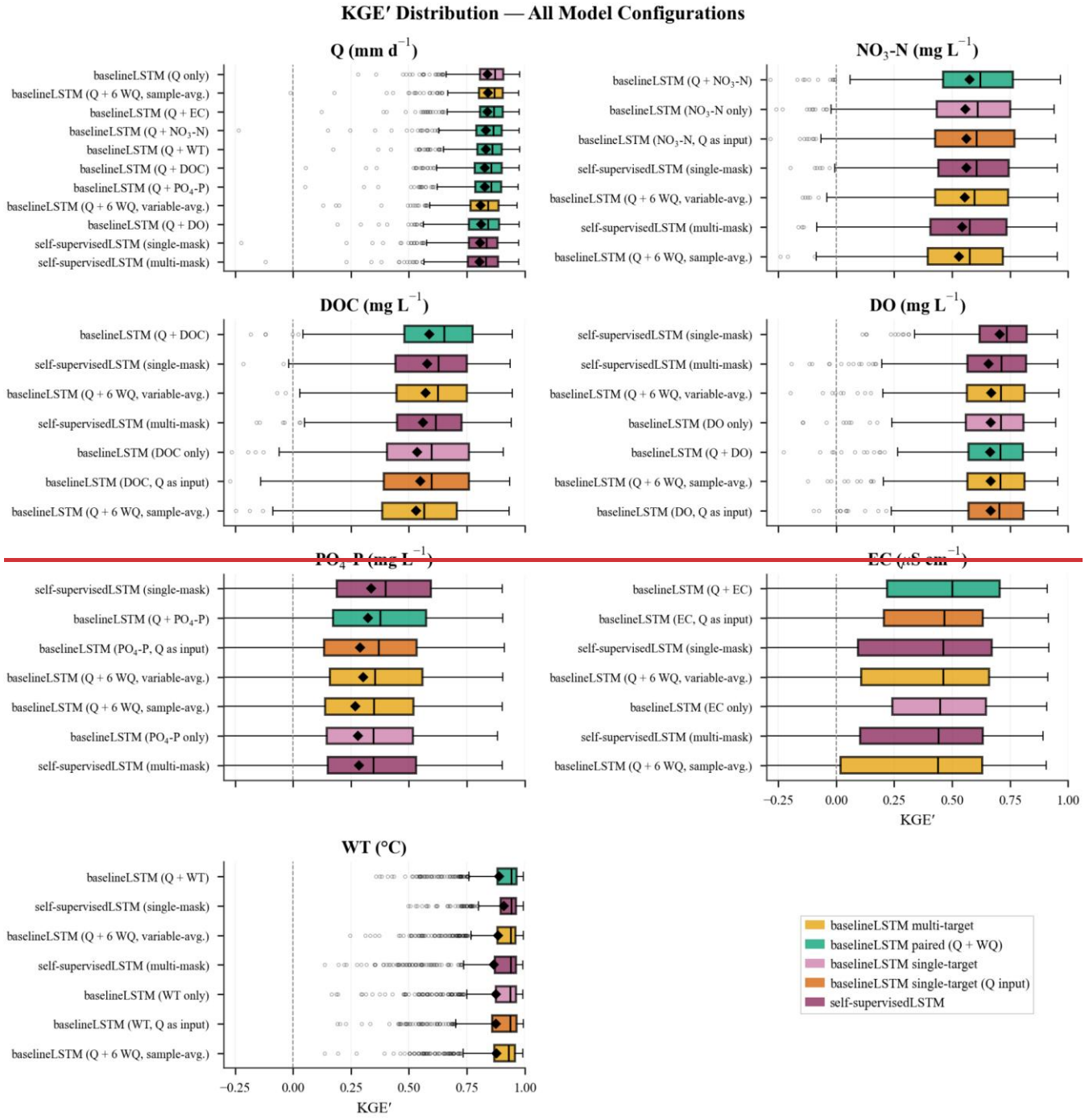

Table B1. Decomposition of KGE′ for all model configurations and target variables on the test period (2010–2019): median over the evaluated catchments (n per variable) of KGE′, the correlation r, the bias ratio β (mean of simulations over mean of observations) and the variability ratio γ (ratio of the coefficients of variation). Medians are computed separately for each component, so the median KGE′ cannot be recomputed from the median components. Within each variable, configurations are ranked by median KGE′; colours indicate the model family as in Table A1. The correlation differs little between configurations

for NO_3-N, DOC, and PO_4-P (range ≤ 0.02), so that differences between configurations arise mainly from the variability ratio γ; for EC, differences in r (0.63–0.72) dominate. All configurations underestimate the variability of the water-quality variables ($\gamma < 1$) except for WT, and PO_4-P is overestimated on average by 15–20 % (β = 1.15–1.20).

Colour	Rank	Model configuration	KGE′	r	β	γ
Q (*n* = 408 catchments)						
	1	baselineLSTM (Q only)	**0.870**	0.949	1.000	0.917
	2	baselineLSTM (Q + 6 WQ, sample-avg.)	0.867	0.948	1.004	0.916
	3	baselineLSTM (Q + NO_3-N)	0.865	0.948	1.004	0.905
	3	baselineLSTM (Q + EC)	0.865	0.948	1.004	0.907
	5	baselineLSTM (Q + WT)	0.863	0.949	1.008	0.910
	6	baselineLSTM (Q + DOC)	0.860	0.947	1.009	0.903
	7	baselineLSTM (Q + PO_4-P)	0.856	0.947	1.008	0.900
	8	baselineLSTM (Q + 6 WQ, variable-avg.)	0.845	0.942	1.018	0.891
	9	self-supervisedLSTM (single-mask)	0.844	0.942	1.018	0.897
	9	self-supervisedLSTM (multi-mask)	0.844	0.942	1.019	0.894
	11	baselineLSTM (Q + DO)	0.843	0.943	1.014	0.895
NO_3-N (*n* = 402 catchments)						
	1	baselineLSTM (Q + NO_3-N)	**0.665**	0.799	1.061	0.804
	1	baselineLSTM (NO_3-N, Q as input)	**0.665**	0.786	1.057	0.829
	3	baselineLSTM (NO_3-N only)	0.656	0.784	1.056	0.826
	4	baselineLSTM (Q + 6 WQ, variable-avg.)	0.646	0.794	1.064	0.781

Colour	Rank	Model configuration	KGE′	*r*	*β*	*γ*
	5	self-supervisedLSTM (single-mask)	0.640	0.795	1.072	0.773
	6	self-supervisedLSTM (multi-mask)	0.635	0.791	1.069	0.768
	7	baselineLSTM (Q + 6 WQ, sample-avg.)	0.606	0.780	1.070	0.759
DOC (*n* = 209 catchments)						
	1	baselineLSTM (Q + DOC)	**0.695**	0.796	1.018	0.813
	2	self-supervisedLSTM (multi-mask)	0.666	0.798	1.025	0.784
	3	baselineLSTM (Q + 6 WQ, variable-avg.)	0.655	0.793	1.023	0.790
	3	self-supervisedLSTM (single-mask)	0.655	0.799	1.026	0.776
	5	baselineLSTM (DOC, Q as input)	0.645	0.792	1.029	0.798
	6	baselineLSTM (DOC only)	0.643	0.781	1.029	0.791
	7	baselineLSTM (Q + 6 WQ, sample-avg.)	0.590	0.792	1.040	0.741
DO (*n* = 402 catchments)						
	1	baselineLSTM (DO, Q as input)	**0.745**	0.824	0.992	0.852
	2	self-supervisedLSTM (multi-mask)	0.744	0.832	0.993	0.839
	3	baselineLSTM (DO only)	0.741	0.835	0.992	0.842
	4	baselineLSTM (Q + 6 WQ, variable-avg.)	0.739	0.823	0.992	0.859
	5	self-supervisedLSTM (single-mask)	0.738	0.833	0.995	0.830

Colour	Rank	Model configuration	KGE′	*r*	*β*	*γ*
	6	baselineLSTM (Q + DO)	0.734	0.807	0.993	0.865
	7	baselineLSTM (Q + 6 WQ, sample-avg.)	0.732	0.835	0.993	0.827
PO_4-P (*n* = 401 catchments)						
	1	baselineLSTM (Q + PO_4-P)	**0.420**	0.653	1.150	0.770
	2	self-supervisedLSTM (single-mask)	0.412	0.654	1.200	0.738
	3	self-supervisedLSTM (multi-mask)	0.410	0.654	1.185	0.730
	4	baselineLSTM (Q + 6 WQ, variable-avg.)	0.402	0.648	1.183	0.752
	5	baselineLSTM (PO_4-P, Q as input)	0.391	0.654	1.193	0.722
	6	baselineLSTM (PO_4-P only)	0.384	0.652	1.183	0.717
	7	baselineLSTM (Q + 6 WQ, sample-avg.)	0.379	0.648	1.204	0.720
EC (*n* = 369 catchments)						
	1	baselineLSTM (Q + EC)	**0.592**	0.717	1.008	0.763
	2	baselineLSTM (EC, Q as input)	0.556	0.693	1.009	0.708
	3	baselineLSTM (Q + 6 WQ, variable-avg.)	0.552	0.658	1.011	0.768
	4	self-supervisedLSTM (single-mask)	0.548	0.671	1.005	0.756
	5	self-supervisedLSTM (multi-mask)	0.538	0.668	1.003	0.751
	6	baselineLSTM (Q + 6 WQ, sample-avg.)	0.521	0.634	1.009	0.770

Colour	Rank	Model configuration	KGE′	*r*	*β*	*γ*
	7	baselineLSTM (EC only)	0.514	0.665	0.996	0.694
WT (*n* = 402 catchments)						
	1	baselineLSTM (Q + WT)	**0.953**	0.988	0.984	1.008
	2	baselineLSTM (WT, Q as input)	0.949	0.988	0.982	1.004
	2	self-supervisedLSTM (multi-mask)	0.949	0.987	0.985	0.995
	4	baselineLSTM (WT only)	0.948	0.988	0.983	0.998
	5	baselineLSTM (Q + 6 WQ, variable-avg.)	0.947	0.987	0.984	0.989
	5	self-supervisedLSTM (single-mask)	0.947	0.987	0.984	0.993
	7	baselineLSTM (Q + 6 WQ, sample-avg.)	0.943	0.986	0.986	0.982

796

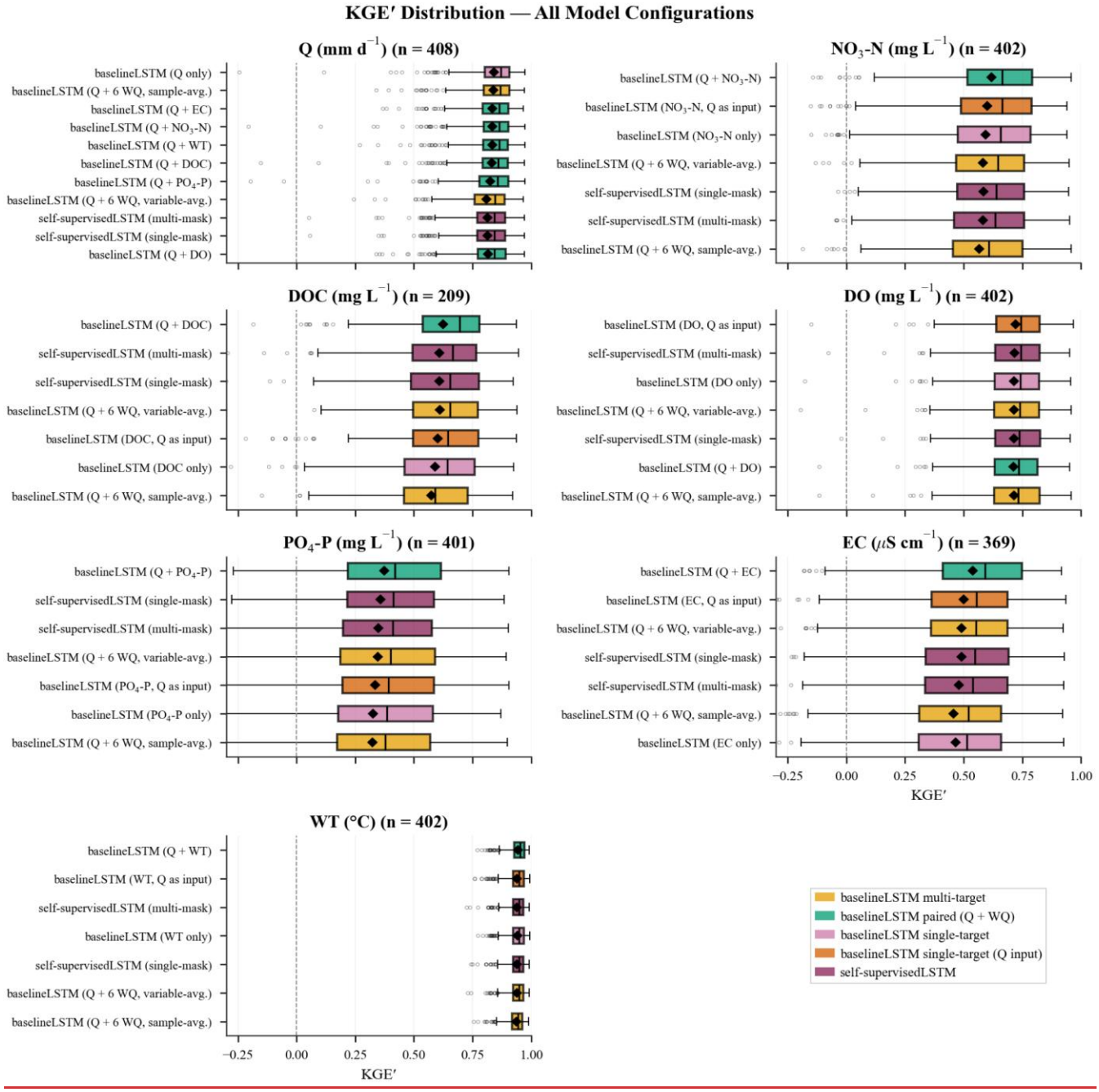

Figure B1. Distribution of test-period KGE′ across the catchments for all model configurations and target variables (2010–2019). Each panel shows one target variable; horizontal boxes correspond to individual model configurations, sorted by ascending median KGE′ (best on top). Colour indicates model family (legend; see Table A1). Box centres mark the median, hinges span the interquartile range (IQR), whiskers extend to 1.5× IQR, black diamonds mark the means, and grey points show individual catchments beyond the whiskers. The dashed vertical line at KGE′ = 0 separates positive from negative scores.


NSE Distribution — All Model Configurations
Q (mm d^{-1})
baselineLSTM (Q + EC)
baselineLSTM (Q only)
baselineLSTM (Q + 6 WQ, sample-avg.)
baselineLSTM (Q + PO_4-P)
baselineLSTM (Q + NO_3-N)
baselineLSTM (Q + WT)
baselineLSTM (Q + DOC)
baselineLSTM (Q + DO)
baselineLSTM (Q + 6 WQ, variable-avg.)
self-supervisedLSTM (multi-mask)
self-supervisedLSTM (single-mask)
NO_3-N (mg L^{-1})
self-supervisedLSTM (single-mask)
baselineLSTM (Q + NO_3-N)
baselineLSTM (NO_3-N, Q as input)
baselineLSTM (Q + 6 WQ, variable-avg.)
baselineLSTM (Q + 6 WQ, sample-avg.)
self-supervisedLSTM (multi-mask)
baselineLSTM (NO_3-N only)
DOC (mg L^{-1})
baselineLSTM (Q + DOC)
self-supervisedLSTM (single-mask)
baselineLSTM (Q + 6 WQ, variable-avg.)
baselineLSTM (DOC only)
baselineLSTM (DOC, Q as input)
self-supervisedLSTM (multi-mask)
baselineLSTM (Q + 6 WQ, sample-avg.)
DO (mg L^{-1})
self-supervisedLSTM (single-mask)
self-supervisedLSTM (multi-mask)
baselineLSTM (Q + 6 WQ, sample-avg.)
baselineLSTM (Q + 6 WQ, variable-avg.)
baselineLSTM (DO only)
baselineLSTM (Q + DO)
baselineLSTM (DO, Q as input)
PO_4-P (mg L^{-1})
self-supervisedLSTM (single-mask)
self-supervisedLSTM (multi-mask)
baselineLSTM (PO_4-P only)
baselineLSTM (PO_4-P, Q as input)
baselineLSTM (Q + PO_4-P)
baselineLSTM (Q + 6 WQ, variable-avg.)
baselineLSTM (Q + 6 WQ, sample-avg.)
EC (µS cm^{-1})
baselineLSTM (Q + EC)
baselineLSTM (EC only)
baselineLSTM (EC, Q as input)
self-supervisedLSTM (single-mask)
self-supervisedLSTM (multi-mask)
baselineLSTM (Q + 6 WQ, variable-avg.)
baselineLSTM (Q + 6 WQ, sample-avg.)
−0.25
0.00
0.25
0.50
0.75
1.00
NSE
WT (°C)
baselineLSTM (Q + WT)
self-supervisedLSTM (single-mask)
baselineLSTM (WT, Q as input)
baselineLSTM (WT only)
self-supervisedLSTM (multi-mask)
baselineLSTM (Q + 6 WQ, variable-avg.)
baselineLSTM (Q + 6 WQ, sample-avg.)
−0.25
0.00
0.25
0.50
0.75
1.00
NSE
baselineLSTM multi-target
baselineLSTM paired (Q + WQ)
baselineLSTM single-target
baselineLSTM single-target (Q input)
self-supervisedLSTM

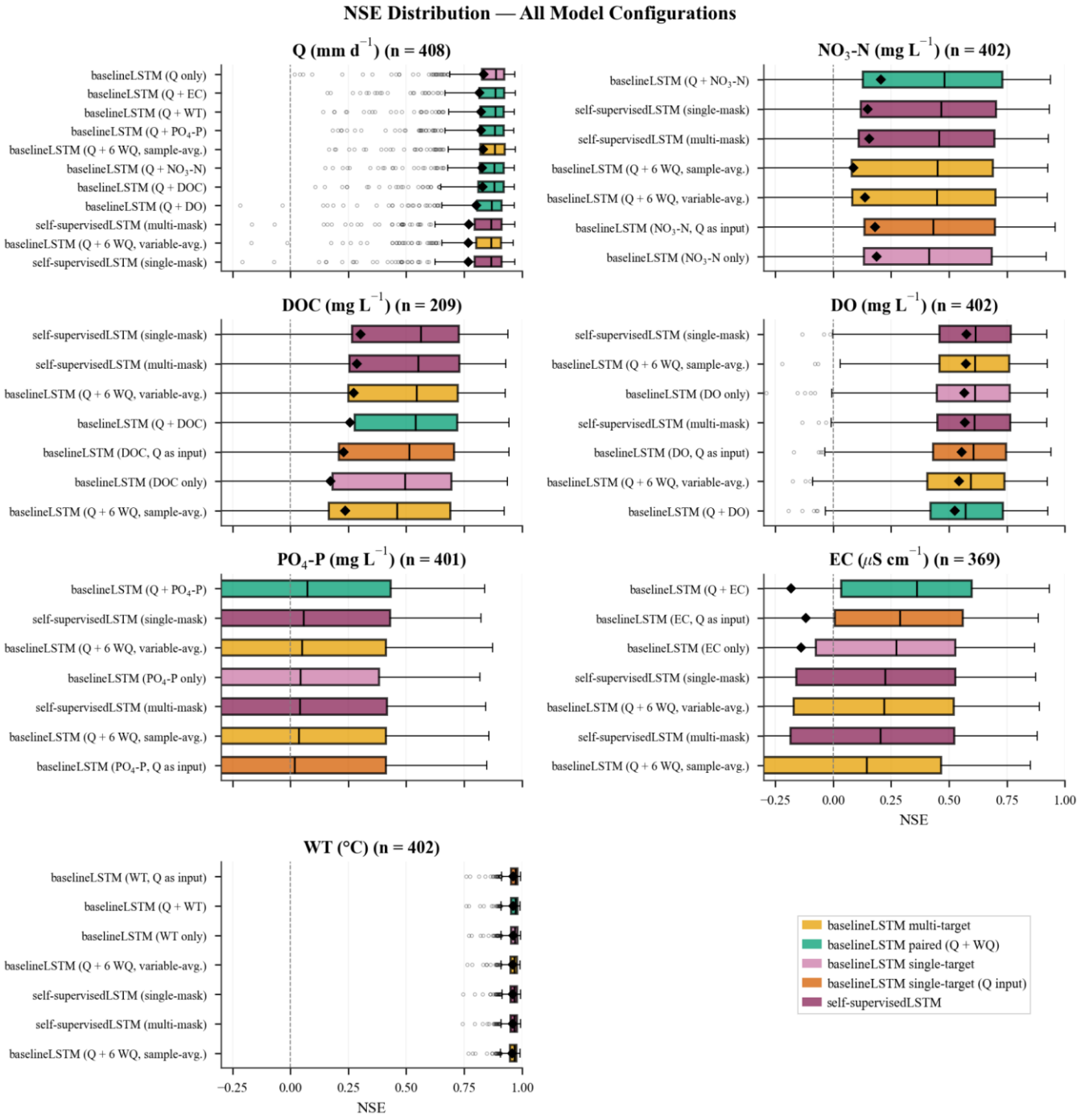

Figure B2. As Fig. B1, but showing distributions of test-period NSE.

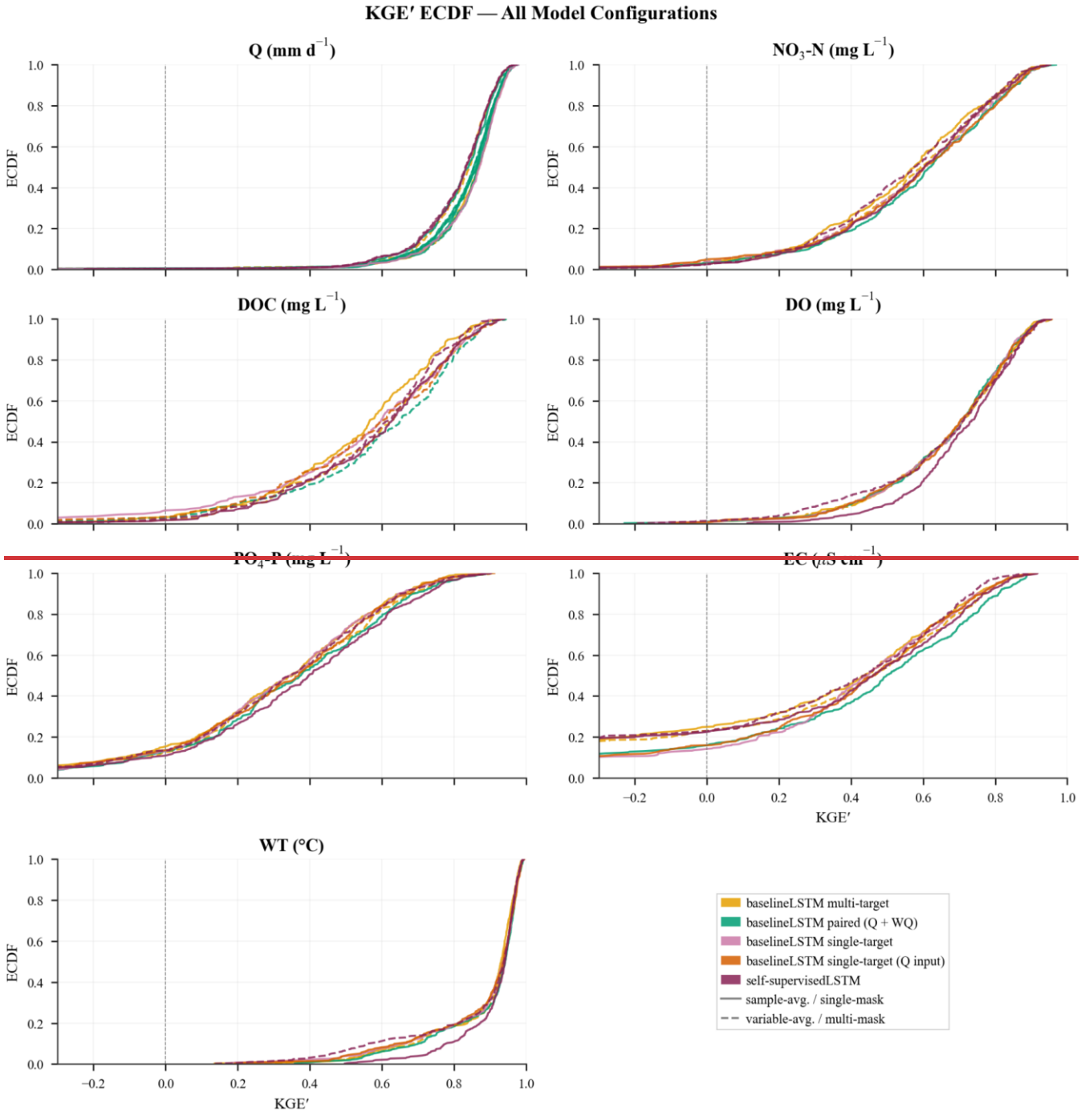
KGE′ ECDF — All Model Configurations
Q (mm d^{-1})
NO_3-N (mg L^{-1})
DOC (mg L^{-1})
DO (mg L^{-1})
PO_4-P (mg L^{-1})
EC (µS cm^{-1})
WT (°C)
ECDF
KGE′
baselineLSTM multi-target
baselineLSTM paired (Q + WQ)
baselineLSTM single-target
baselineLSTM single-target (Q input)
self-supervisedLSTM
sample-avg. / single-mask
variable-avg. / multi-mask

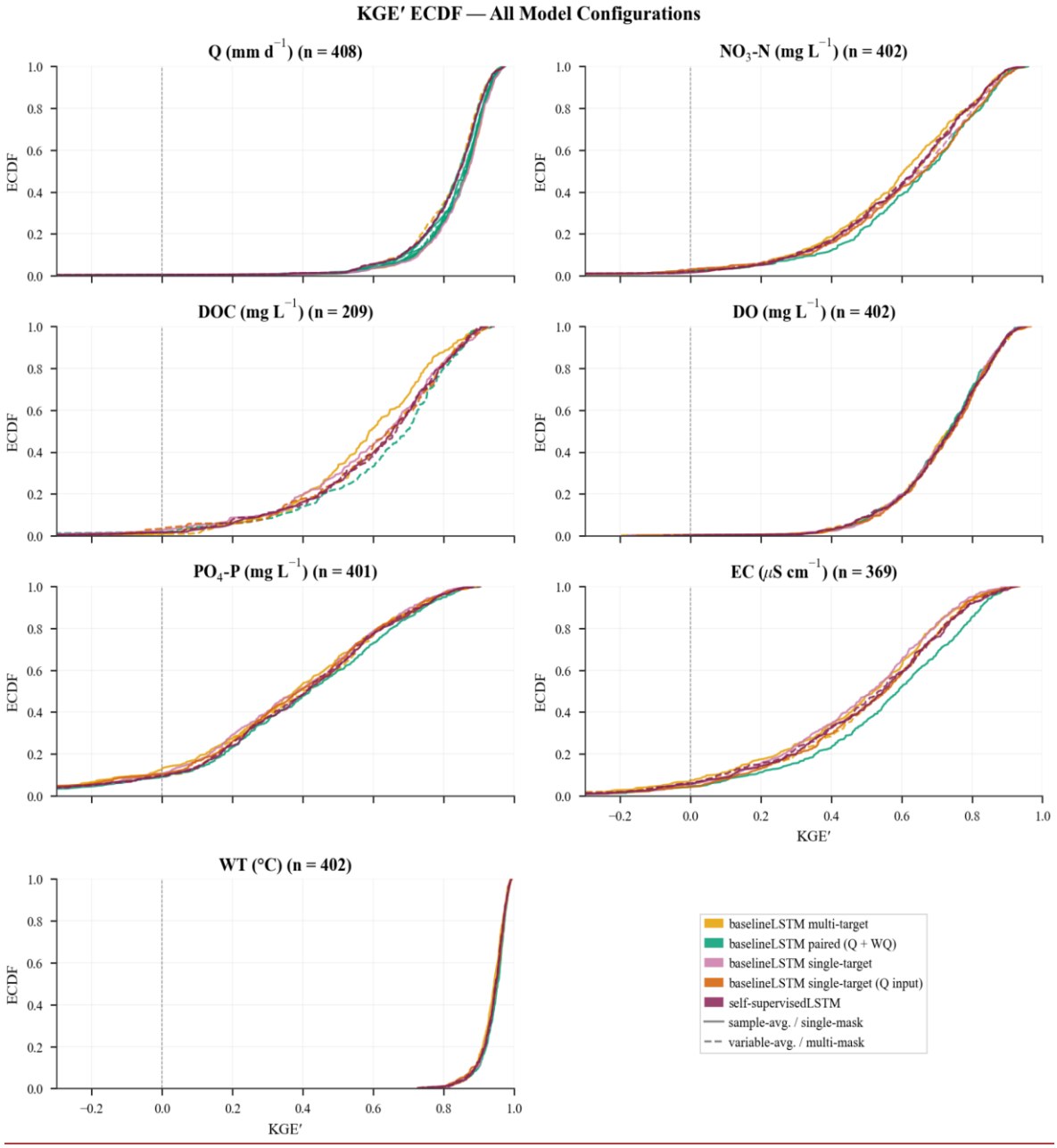

Figure B3. Empirical cumulative distribution functions (ECDFs) of test-period KGE′ across the evaluated catchments (*n* per panel) for all model configurations and target variables (2010–2019). Each panel shows one target variable; one ECDF curve per model configuration. Line colour indicates model family (legend; see Table A1). Within the multi-target $_{\text{baseline}}$LSTM and the $_{\text{self-supervised}}$LSTM families, solid lines denote the sample-averaged loss and single-mask scenario, dashed lines the variable-averaged loss and multi-mask scenario, respectively. The dashed vertical line at KGE′ = 0 separates positive from negative scores.

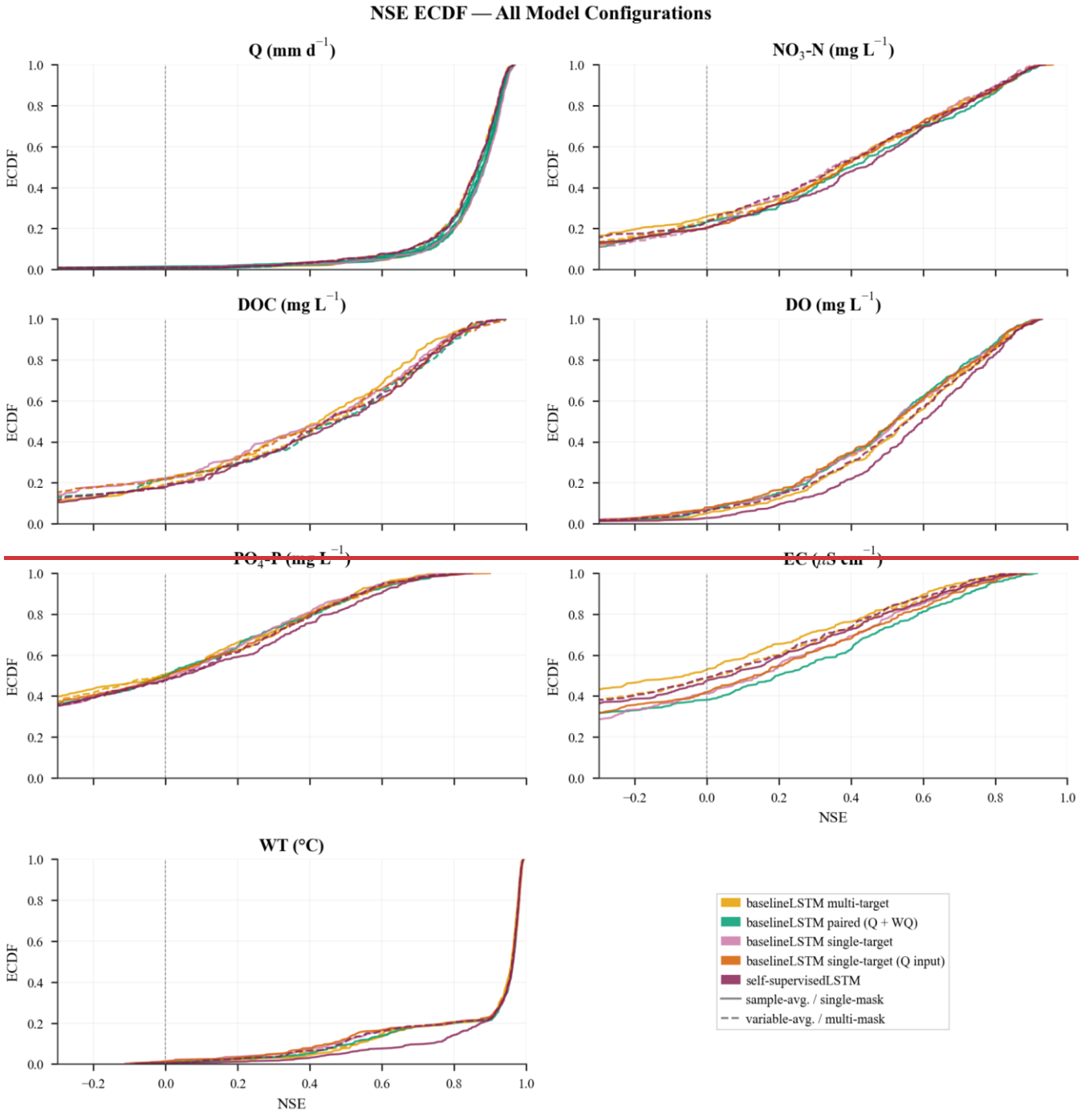
NSE ECDF — All Model Configurations
Q (mm d^{-1})
NO$_3$-N (mg L^{-1})
DOC (mg L^{-1})
DO (mg L^{-1})
PO$_4$-P (mg L^{-1})
EC (µS cm^{-1})
WT (°C)
ECDF
NSE
baselineLSTM multi-target
baselineLSTM paired (Q + WQ)
baselineLSTM single-target
baselineLSTM single-target (Q input)
self-supervisedLSTM
sample-avg. / single-mask
variable-avg. / multi-mask

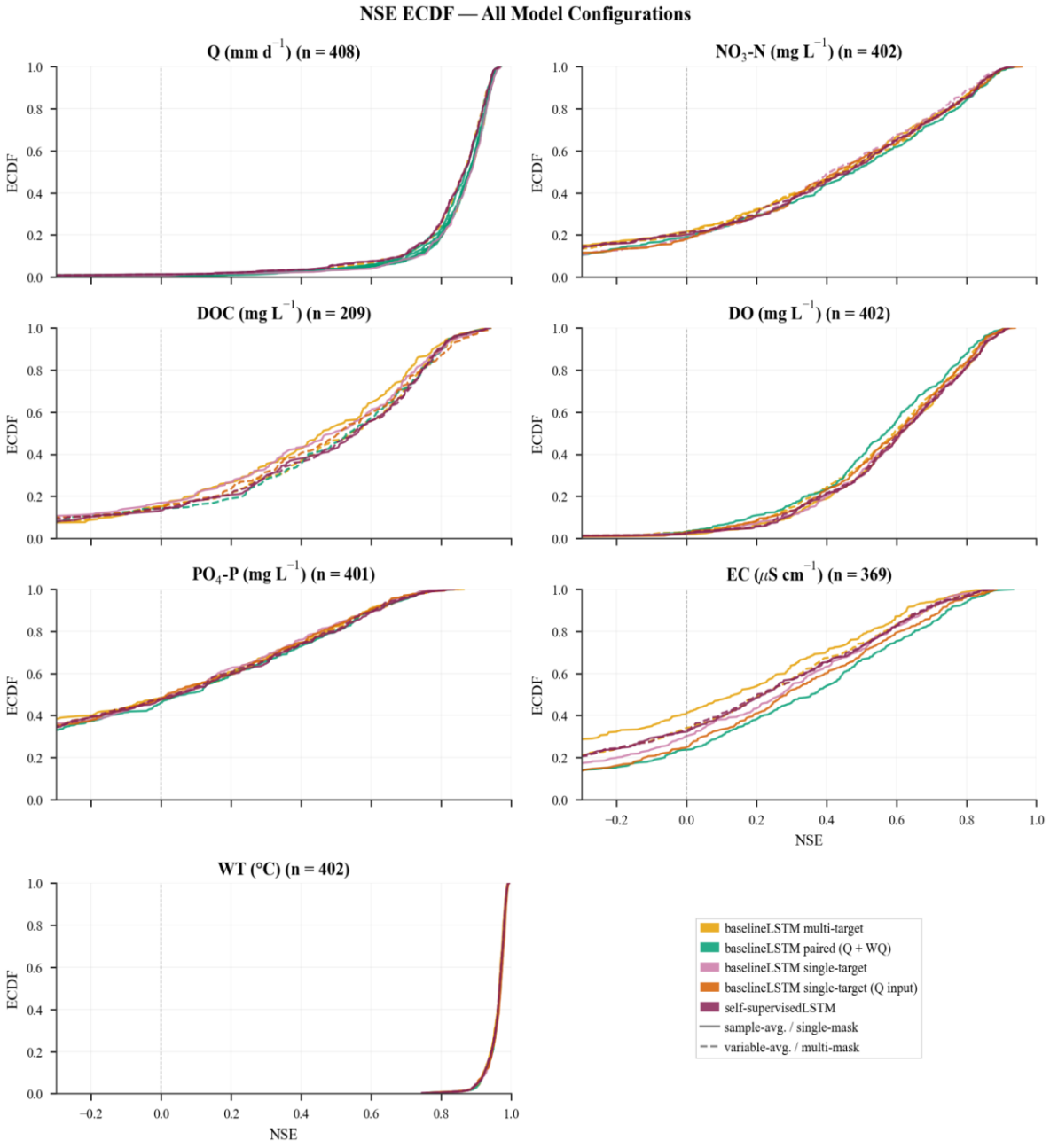

Figure B4. As Fig. B3, but showing ECDFs of test-period NSE.

Appendix C: Data distribution

Appendix C gives details ~~to~~on all model inputs.

Table C1. Overview of all data used in the ~~modeling~~modelling process including ~~variables~~variable descriptions and median and maximum sample count per variable and sample split period. Medians and maxima refer to the catchments with at least one sample of the respective variable and period (DOC: 282 training, 315 testing; EC: 374 training, 407 testing; all other variables: 408).

			Per-catchment sample count			
			Training		Testing	
Variable	Unit	Description	Median	Max	Median	Max
CAMELS-DE						
Catchment attributes						
Area	km²	Catchment area	–	–	–	–
Elevation	m a.s.l.	Mean catchment elevation	–	–	–	–
Clay fraction	%	Mean clay content (0–30 cm depth)	–	–	–	–
Sand fraction	%	Mean sand content (0–30 cm depth)	–	–	–	–
Silt fraction	%	Mean silt content (0–30 cm depth)	–	–	–	–
Artificial surfaces	%	Fraction of artificial/urban land cover	–	–	–	–
Agricultural areas	%	Fraction of agricultural land cover	–	–	–	–
Forests & semi-natural	%	Fraction of forest and semi-natural land cover	–	–	–	–
Wetlands	%	Fraction of wetland land cover	–	–	–	–
Water bodies	%	Fraction of water body land cover	–	–	–	–
Climatic indices						

Mean precipitation	mm d^{-1}	Long-term mean daily precipitation	–	–	–	–
Precipitation seasonality	–	Seasonality index of precipitation	–	–	–	–
Snow fraction	–	Fraction of precipitation falling as snow	–	–	–	–
High precipitation frequency	d yr^{-1}	Frequency of high-precipitation days	–	–	–	–
Low precipitation frequency	d yr^{-1}	Frequency of low-precipitation days	–	–	–	–
High precipitation duration	d	Mean duration of high-precipitation events	–	–	–	–
Low precipitation duration	d	Mean duration of low-precipitation events	–	–	–	–
Meteorological forcing						
Precipitation (mean)	mm d^{-1}	Daily mean areal precipitation	daily	daily	daily	daily
Precipitation (min)	mm d^{-1}	Daily minimum areal precipitation	daily	daily	daily	daily
Precipitation (max)	mm d^{-1}	Daily maximum areal precipitation	daily	daily	daily	daily
Humidity	%	Daily mean relative humidity	daily	daily	daily	daily
Global radiation	W m^{-2}	Daily mean global radiation	daily	daily	daily	daily
Temperature (mean)	°C	Daily mean air temperature	daily	daily	daily	daily
Temperature (min)	°C	Daily minimum air temperature	daily	daily	daily	daily
Temperature (max)	°C	Daily maximum air temperature	daily	daily	daily	daily
Streamflow						

	Specific discharge	mm d^{-1}	Observed specific discharge	daily	daily	daily	daily
QUADICA							
Nutrients							
	NO_3-N	mg L^{-1}	Nitrate-nitrogen concentration	109	273	105	~~1,164~~318
	PO_4-P	mg L^{-1}	Orthophosphate-phosphorus concentration	~~101~~100	273	103	234
Organic Carbon							
	DOC	mg L^{-1}	Dissolved organic carbon concentration	~~65~~88	252	~~24~~29	216
Physical properties							
	WT	°C	Water temperature	~~113~~112	885	105	~~1,175~~234
	EC	µS cm^{-1}	Electrical conductivity	~~102~~110	3,~~327~~347	~~102~~103	2,~~964~~966
Dissolved gases							
	DO	mg L^{-1}	Dissolved oxygen concentration	~~111~~110	3,392	105	3,041

Appendix D: Uncertainty estimation

Appendix D presents a paired bootstrap analysis comparing the baseline model family that uses Q as an input with the one that uses Q as a co-target. Comparing models by their median performance across hundreds of catchments reduces each performance distribution, itself already an aggregate, to a single value. This common practice discards information on where and why models differ and can lead to misinterpretation. The outcome also depends on the choice of metric (e.g. KGE′, NSE, RMSE, r) and of summary statistic (e.g. mean, median). To quantify the uncertainty of the central result of this study, the effect of using Q as a co-target rather than as an input, we conducted a paired bootstrap analysis with 10,000 resamples for each model pair. Each resample draws n catchments with replacement, where n is the number of evaluated catchments per variable, and the same catchments are used for both models. For each resample, we compute (i) the difference between the median KGE′ of the two models and (ii) the median of the per-catchment KGE′ differences. This yields sampling distributions of both measures that reflect their dependence on the set of evaluated catchments. The resulting values and their 95 % confidence intervals are given in Table D1.

Table D1. Paired bootstrap comparison of the $_{\text{baseline}}$LSTM paired with Q as co-target and the $_{\text{baseline}}$LSTM single-target with Q as input on the test period (2010–2019). Coloured squares indicate the model family (Table A1). Both models are evaluated as the ensemble mean (N = 5) on a shared evaluation set per variable. This set contains only days on which both models produce a simulation (single-target (+ Q in) gives no simulation when observed Q is missing in the 365-day input sequence) and only catchments with WQ samples in both the training and test periods; n is the resulting number of catchments. ΔKGE′ is always Q as co-target minus Q as input, so positive values favour Q as a co-target. "Difference of medians" is the median KGE′ of the paired model minus the median KGE′ of the single-target (+ Q in) model. "Median of per-catchment differences" is the median of the KGE′ differences computed catchment by catchment. The last column gives the number of catchments in which each model has the higher KGE′.

Variable	■ Median KGE′ Q as co-target (paired)	■ Median KGE′ Q as input (single-target + Q in)	ΔKGE′ difference of medians [95 % CI]	ΔKGE′ median of per-catchment differences [95 % CI]	Catchments better (■ co-target / ■ input)
NO_3-N (402)	0.665	0.665	0.001 [−0.013, 0.025]	0.012 [0.006, 0.018]	237 / 165
PO_4-P (401)	0.420	0.391	0.029 [0.002, 0.052]	0.027 [0.017, 0.039]	264 / 137
DO (402)	0.734	0.745	−0.011 [−0.023, −0.001]	−0.008 [−0.012, −0.003]	160 / 241
DOC (209)	0.695	0.645	0.050 [0.021, 0.081]	0.021 [0.007, 0.031]	126 / 83
EC (369)	0.592	0.556	0.036 [0.014, 0.059]	0.038 [0.026, 0.052]	248 / 121
WT (402)	0.953	0.949	0.004 [0.000, 0.008]	0.003 [0.001, 0.004]	233 / 168